Elevated temperature mechanical properties of cold-rolled steel sheets and cold-formed steel sections

M. Rokilan and M. Mahendran

Queensland University of Technology (QUT), Brisbane, Australia

Abstract: Cold-formed steel (CFS) is increasingly used in building construction in many countries due to its lightweight and fast and easy construction characteristics. However, its fire resistance is not well understood, which may restrict its applications. For fire design purposes, a good knowledge of the elevated temperature mechanical properties of CFS is essential. Although several useful studies have been conducted on the mechanical properties of CFS, the elevated temperature reduction factors vary significantly among them while no predictive equation is available to calculate the proportional limit stress of CFS at elevated temperatures. Moreover, they also show significant variations between the elevated temperature reduction factors of cold-rolled steel sheets and CFS sections. In this research, low and high strength cold-rolled steel sheets and high strength CFS lipped channel sections and floor decks were tested in the temperature range of 20 to 700 ^{o}C under isothermal conditions to determine the reductions in their mechanical properties. Predictive equations given in AS/NZS 4600 for yield strength and Young's modulus were verified, and new predictive equations for ultimate strength, stress at 2% total strain, 0.05% proof stress and proportional limit stress were proposed. Finally, a two-stage stress-strain model was proposed to accurately predict the stress-strain curves of CFS at ambient and elevated temperatures.

Keywords: Mechanical properties; Elevated temperatures; Reduction factors; Two-stage stress-strain model; Cold-rolled steel sheets; Cold-formed steel sections

**Corresponding author's email address:* m.mahendran@qut.edu.au

1. Introduction

Mechanical properties and stress-strain characteristics of cold-formed steels (CFS) at elevated temperatures are essential parameters for predicting the capacities of CFS structural elements at elevated temperatures. However, mechanical property tests are not easy to conduct at elevated temperatures compared to those at ambient temperature. The CFS manufacturers rarely provide elevated temperature mechanical properties of their products while most of them provide only the ambient temperature mechanical properties. Therefore it is necessary to determine the relationship between the ambient and elevated temperature mechanical properties of CFS.

Several studies have been conducted on elevated temperature mechanical properties of cold-rolled steel sheets and cold-formed steel sections. Ranawaka and Mahendran [1], Kankanamge and Mahendran [2] and Landesmann et al. [3] investigated the elevated temperature mechanical properties of cold-rolled steel sheets. On the other hand, McCann et al. [4], Imran et al. [5] and Li and Young [6] investigated the elevated temperature mechanical properties of cold-formed steel hollow sections while Craveiro et al. [7] and Kesawan et al. [8] investigated the elevated temperature mechanical properties of cold-formed steel lipped channel and hollow flange channel sections, respectively. Also, many design standards such as AS/NZS 4600 [9], AS/NZS 2327 [10], BS 5950-Part 8 [11] and Eurocode 3 Part 1-2 [12] provide elevated temperature mechanical properties of cold-formed and hot-rolled steels. Although many research papers and standards provide elevated temperature mechanical property reduction factors to be used with ambient temperature mechanical properties, the reduction factors are not consistent, and any similarities among them are difficult to identify. Further, the elevated temperature mechanical property reduction factors obtained for hollow sections [5] and hollow flange channel sections [8] were considerably higher than those obtained for cold-rolled steel sheets [2]. This might have been due to the effects of cold-forming process and raises the question whether the elevated temperature mechanical properties of cold-rolled steel sheets can be used in the fire design of both open and closed CFS sections.

Kankanamge and Mahendran [13] showed that CFS exhibits a highly nonlinear stress-strain behaviour at elevated temperatures, which influences the moment capacities of CFS beams predicted using ambient temperature design rules with elevated temperature mechanical properties. This is recognized in AS/NZS 4600 [9], which limits the use of ambient temperature design rules with elevated temperature mechanical properties for CFS members based on the

ratio of proportional limit stress to yield strength. However, predictive equations are not available to determine the proportional limit stress to yield strength ratio for CFS at elevated temperatures. Moreover, many researchers and standards proposed a simplified one-stage stress-strain model for CFS at ambient and elevated temperatures based on Ramberg and Osgood [14] stress-strain model. However, such one-stage models give high strain hardening for the material with high nonlinearity (between proportional limit stress and yield strength) and low strain hardening for the material with low nonlinearity, which is not true for all CFS materials. Hence, it is necessary to formulate a two-stage model or a multi-stage model to accurately predict the stress-strain curves of CFS. Gardner and Yun [15] proposed a two-stage stress-strain model to represent the stress-strain behaviour of CFS at ambient temperature. However, its suitability for CFS at elevated temperatures is not known.

An experimental study was therefore undertaken to investigate the elevated temperature mechanical properties of cold-rolled steel sheets and cold-formed steel sections, such as 0.2% proof stress or yield strength, Young's modulus, ultimate strength, proportional limit stress, stress at 2% total strain, 0.05% proof stress, ultimate strain and fracture strain. The accuracy of predictive equations available for some mechanical properties is assessed while new predictive equations are developed for others. A two-stage stress-strain model is also proposed to accurately predict the stress-strain behaviour of CFS based on the ambient temperature stress-strain model proposed by Gardner and Yun [15]. This paper presents the details of this experimental study and its results.

2. Experimental study

2.1. Test coupon and test method

Uniaxial tensile tests were conducted to determine the elevated temperature mechanical properties of 0.8 mm and 1.0 mm low strength (G300) and 0.55 mm, 0.75 mm and 0.95 mm high strength (G550) cold-rolled steel sheets. They were also conducted for 0.75 mm and 1.2 mm high strength (G550) CFS lipped channel sections and 0.75 mm and 1.0 mm high strength (G550) CFS floor decks.

Non-proportional type tensile coupons were prepared as per the dimensions given in AS 1391 [16] and AS 2291 [17] (Fig. 1). They were selected over proportional type coupons to keep a constant gauge length (50 mm), which reduces the calibration requirements of extensometer. Non-proportional type coupons do not provide exact fracture strain because fracture strain

reduces as the gauge length increases. However, the minimum fracture strain to satisfy the ductility requirement is also given for 50 mm gauge length as per AS/NZS 4600 [9].

Tensile coupons were extracted in the longitudinal direction of cold-rolled sheets and cold-formed sections using the water cutting method as recommended by Imran et al. [5]. Fig. 2 shows the CFS floor deck and lipped channel sections after the extraction of tensile coupons. Extracted coupons were subjected to a chemical etching process to remove the corrosion prevention coating. Removal of coating allows the measurement of base metal thickness and reduces the extensometer slip. The coupons were dipped into diluted HCL and kept until the coating had been removed completely. They were then washed using distilled water followed by acetone. The base metal thickness and the width of the coupons were measured at three locations within the gauge length using a Vernier calliper. Average measured values of base metal thickness and width were used in the mechanical property calculations.

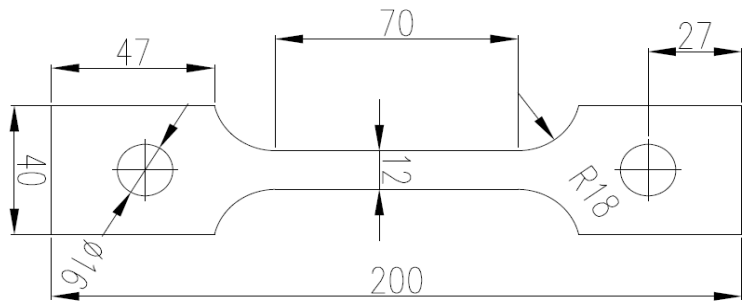

Fig. 1. Dimensions of tensile coupons

The tensile coupons were tested in a temperature range of ambient temperature to 700 ^{0}C under isothermal/steady state conditions. The anisothermal/transient state test method is more realistic, but it has some drawbacks. Firstly, the stress-strain curve cannot be obtained directly, instead it has to be derived from the temperature-strain curves. Hence the accuracy of the stress-strain curve depends on the number of tested samples [18]. Secondly, the temperature effect on the extensometer is small in the steady-state method as it is inserted just before the load application begins whereas the extensometer is kept inside the furnace in the transient test method. Finally, the applied load has to be continuously adjusted as it changes due to the thermal expansion of the coupon, which may cause some errors. The same reasons are given by other researchers [2, 3, 5, 7, 8], who also used the steady-state method. Most importantly, AS 2291 [17] discusses only the test process relevant to the steady-state test method.

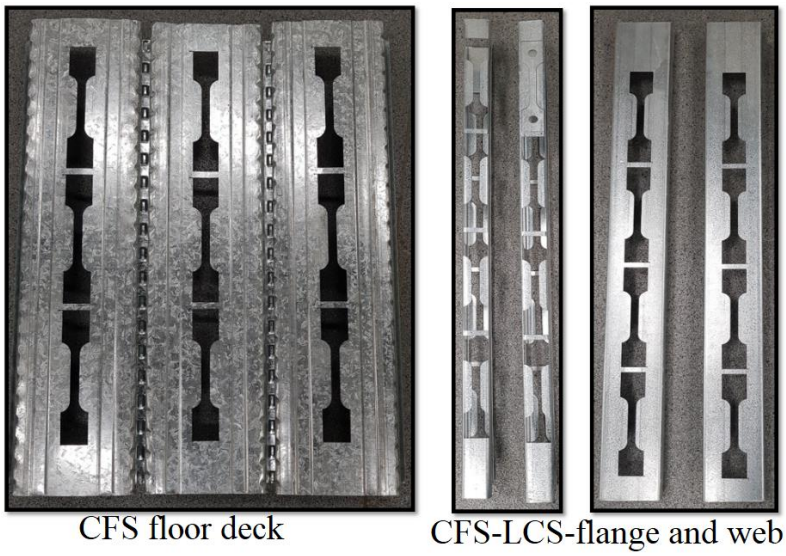

Fig. 2. CFS floor deck and lipped channel sections after the extraction of coupons

2.2. Test set-up and procedure

The elevated temperature tensile coupon test facility in the QUT Wind and Fire laboratory was used to test the coupons at both ambient and elevated temperatures. Fig. 3 shows the tensile test set-up. The test set-up consisted of a 100 kN Instron testing machine, an electric furnace with three independently controllable heating zones, a rod type high-temperature extensometer with 50 mm gauge length and straight type chisel, a heat control unit and a rod type thermometer. The Instron testing machine was connected to a Bluehill software system for data acquisition purposes and to control the load application process.

The tensile coupons were attached to steel jaws fixed to the top and bottom loading shafts using 16 mm diameter stainless steel bolts. Suitable flat washers were used on both sides of the tensile coupon to avoid eccentricity as the jaw slot size (3 mm) was larger than the coupon thickness. Then a preload of approximately 250 N was applied, and the extensometer was attached. The initial extensometer reading was kept as much as close to zero. After the initial set-up, tensile coupon was loaded up to 50% of the expected yield load using a displacement control method (1mm/min) [5,8] and then unloaded. The loading and unloading process was conducted three times for each coupon and the Young's modulus was calculated for each loading process and compared with the nominal value of 200 GPa. This procedure was conducted to ensure the vertical and horizontal alignments of the attached coupon. Moreover, the elevated temperature Young's modulus reduction factors were calculated based on the corresponding ambient temperature Young's modulus obtained from the preloading process.

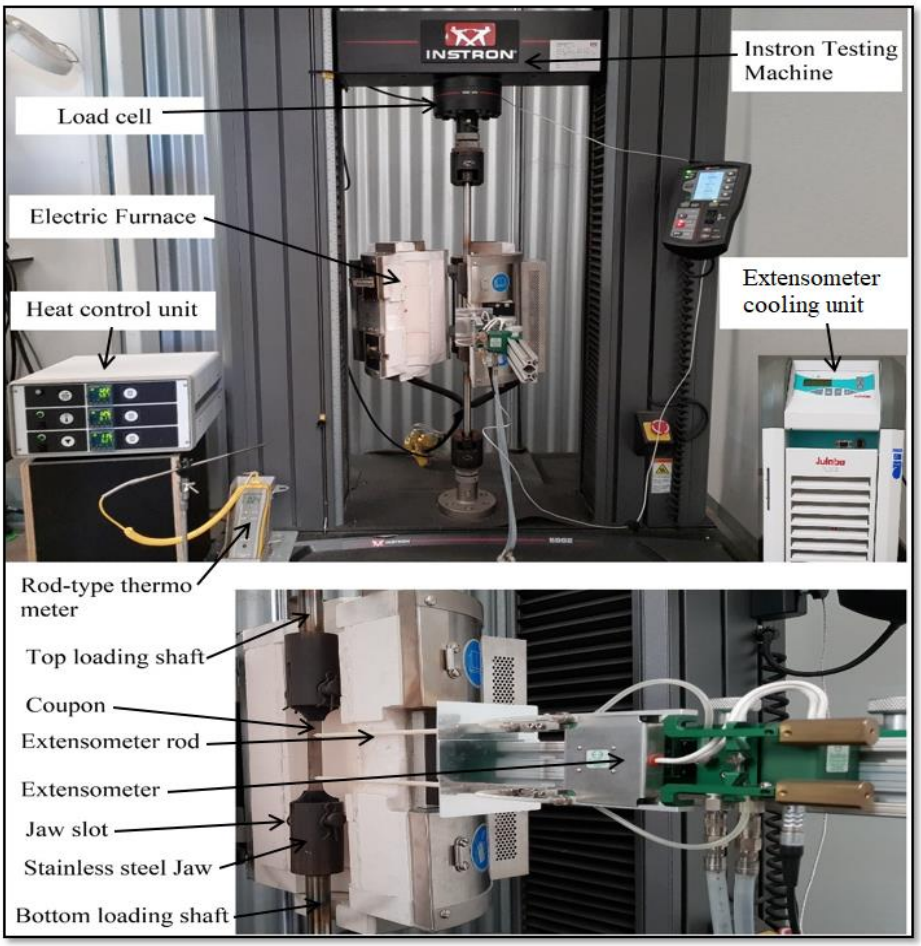

Fig. 3. Elevated and ambient temperature tensile test set-up

After the initial set-up, the extensometer was removed, and the target temperatures of the three different zones were set using the temperature control unit. The target temperature of the top zone was set lower than the test temperature while those of the middle and bottom zones were set higher than the test temperature as heat flows upwards in the furnace. However, the target temperatures were adjusted based on the rod-type thermometer reading throughout the test to maintain the same temperature within the coupon's gauge length. Also, a tensile load of 100-150 N was maintained in the test to ensure that the initial alignment was kept unchanged during elevated temperature loading. The coupon was kept for about 15 min at the test temperature to ensure a uniform temperature across the cross-section as specified in AS 2291 [17]. In the final stage, the extensometer was attached to the coupon with a friction force of 3 to 4 N, and was kept cool using a cooling device. Finally the tensile load was applied to the coupon using a displacement control method (1 mm/min) until its failure. The corresponding strain rate is 0.000238/s, which is within the range of 0.0002 to 0.0008/s given in AS 2291 [17].

3. Elevated and ambient temperature mechanical properties

Elevated temperature mechanical properties of cold-rolled steel sheets are discussed first in this section since cold-formed steel floor decks and lipped channel sections showed similar elevated temperature reduction characteristics as cold-rolled steel sheets. In this study, tensile coupons were extracted from five types of cold-rolled sheets and tested to failure at ambient and elevated temperatures. Their ambient and elevated temperature mechanical properties such as yield strength (0.2% proof stress), stress at 2% total strain, 0.05% proof stress, Young's modulus, ultimate strength, ultimate strain and fracture strain (Fig. 4) were determined using the experimental stress-strain curves. The average mechanical properties were obtained from at least three and two coupon tests for ambient and elevated temperatures, respectively. The average mechanical properties of cold-rolled steel sheets were used first to derive the predictive equations of elevated temperature mechanical property reduction factors. The derived predictive equations were then compared with the elevated temperature mechanical property reduction factors of cold-formed steel floor decks and lipped channel sections.

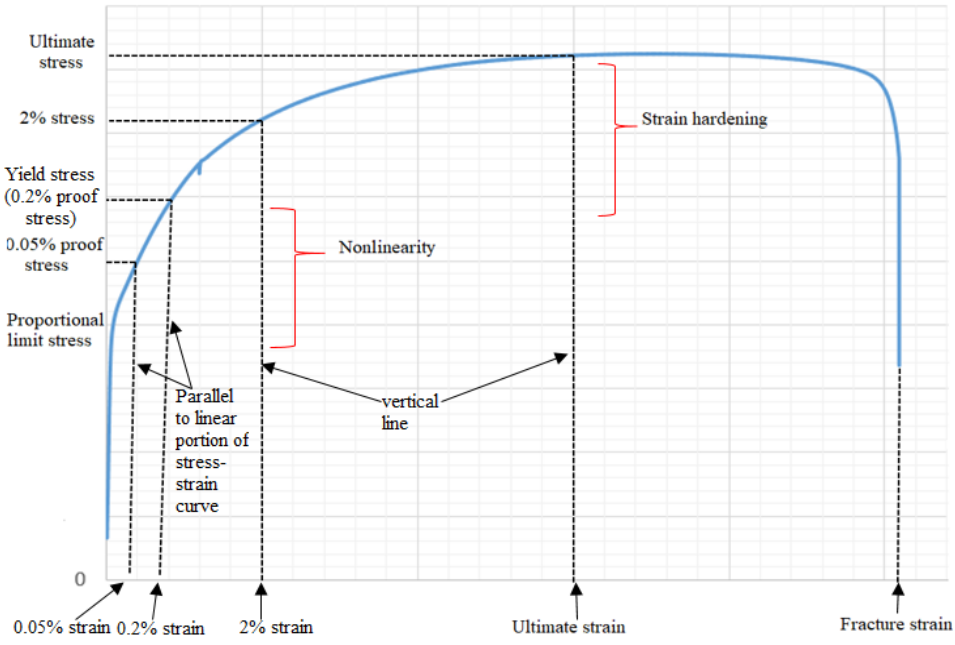

Fig. 4. Definitions of mechanical properties

3.1. Stress-strain curves

The stress-strain curve is the first outcome of tensile coupon tests, and is used to determine the mechanical properties. The stress-strain curves given in Figs. 5 and 6 are engineering stress-strain curves of cold-rolled steel sheets (high strength steel G550 and low strength steel G300

with varying thicknesses) obtained from this study. Stress is calculated as the ratio of applied load to the initial area, while strain is calculated as the ratio of elongation to the initial length in these curves. The similarity among the stress-strain curves of different specimens at a given temperature, steel grade and thickness (Figs. 5 and 6) exhibits the accuracy of test results. At some temperatures, the stress-strain curves show slight deviations due to the differences in the amount of cold work and chemical composition.

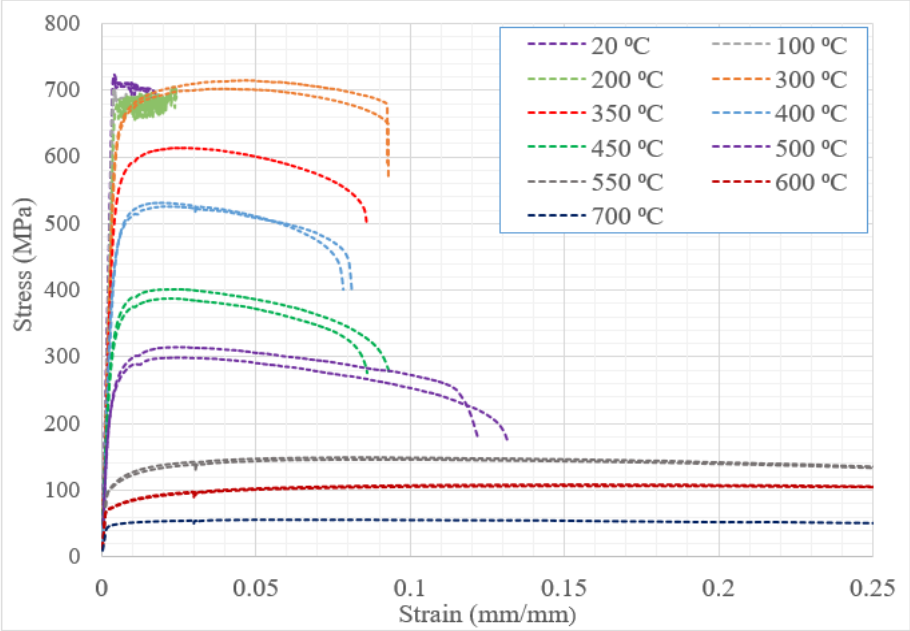

a. G550 - 0.55 mm

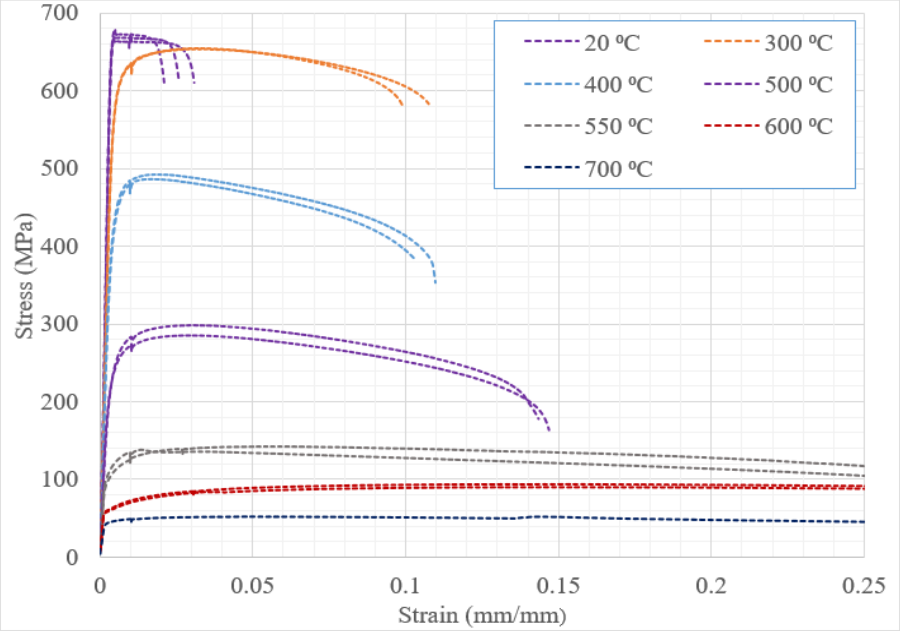

b. G550 - 0.75 mm

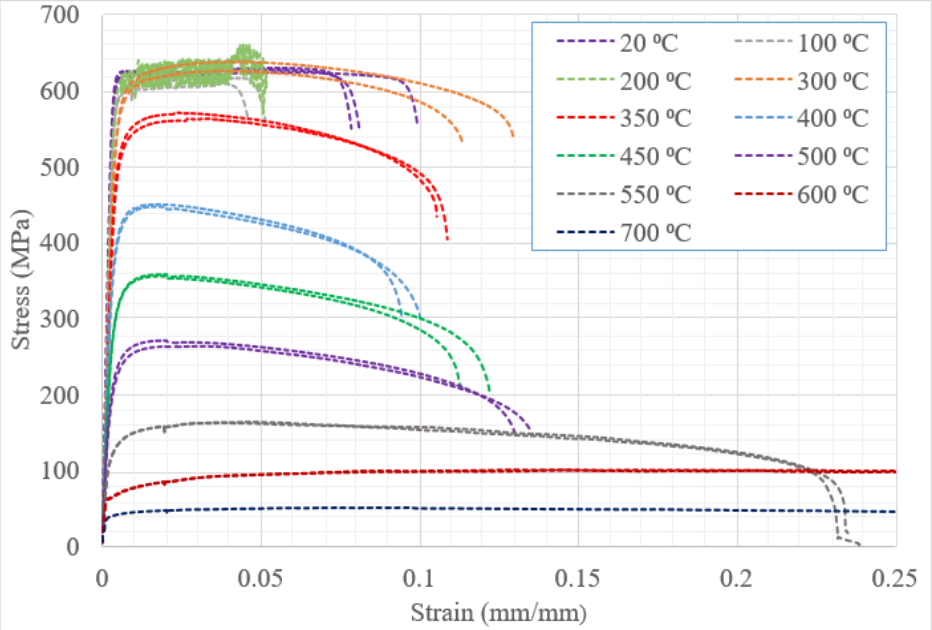

c. G550 - 0.95 mm

Fig. 5. Experimental stress-strain curves of high strength steels (HSS)

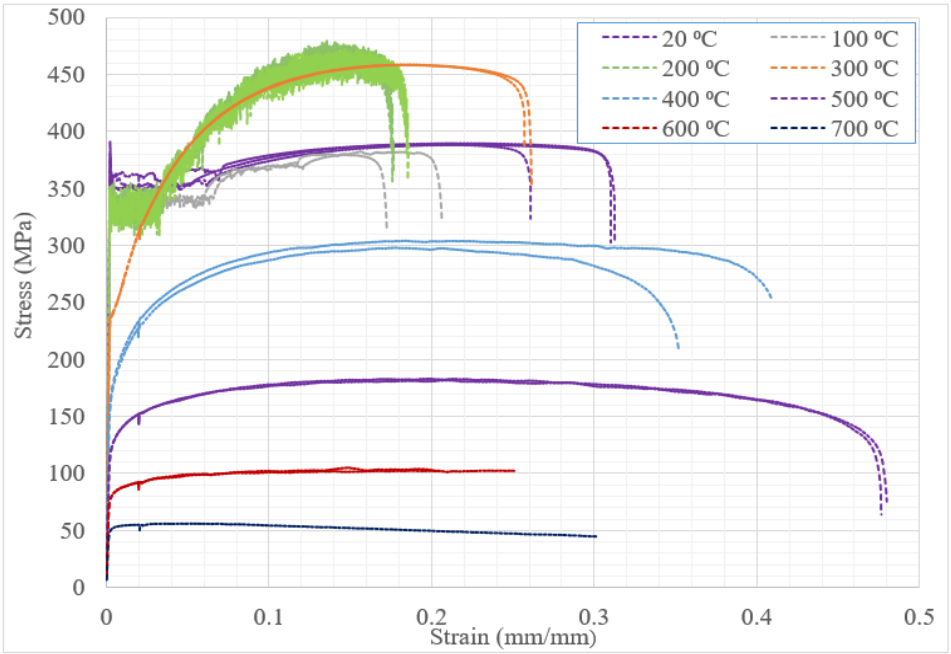

a. G300 – 0.8 mm

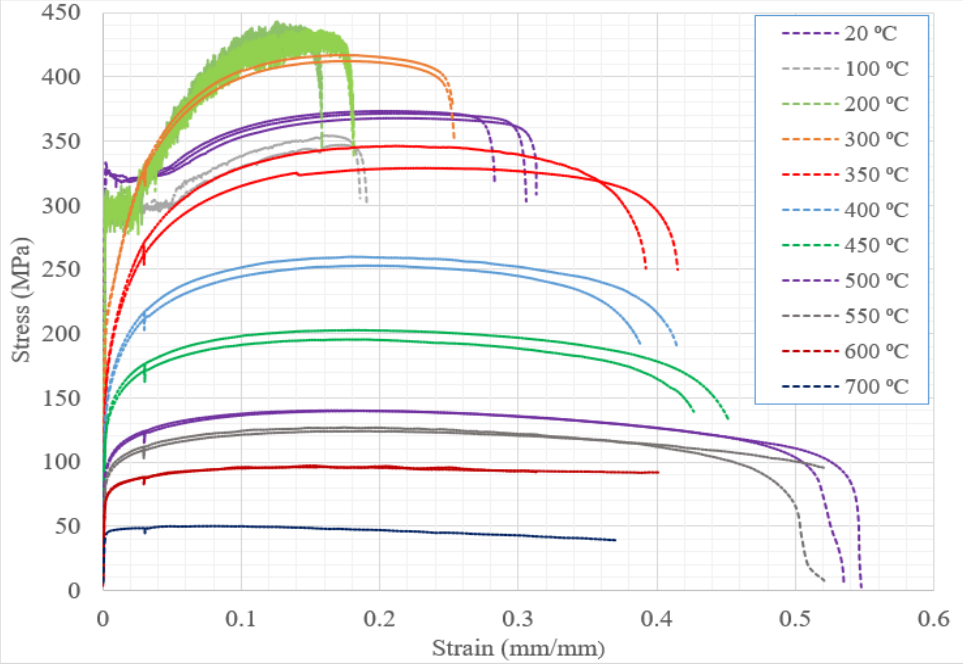

b. G300 – 1.0 mm

Fig. 6. Experimental stress-strain curves of low strength steels (LSS)

3.2. Yield strength

As shown in Figs. 5 and 6, the yielding point of steel can be either sharp yielding or gradual yielding. The yield strength calculation is straightforward in the case of sharp yielding while it is slightly complicated for gradual yielding. For gradual yielding, different standards use different concepts to define the yield strength. However, the 0.2% proof stress, commonly used and adopted in AS/NZS 4600 [9] was used in this study. Table 1 and Fig. 7 show the yield strengths obtained from the measured stress-strain curves and the elevated temperature yield strength reduction factors calculated as the ratios of the ambient temperature yield strength. As shown in Fig. 7, high strength steels (HSS) show a slight drop in yield strength up to 300 ^{0}C, and then the reduction rate increases up to 600 ^{0}C while the yield strength of low strength steels (LSS) reduces slightly up to 200 ^{0}C, and then the reduction rate increases up to 700 ^{0}C. It is interesting to note that although the yield strength reduction factor of LSS is much lower than that of HSS at 300 ^{0}C, it is higher than that of HSS after 500 ^{0}C. Moreover, the yield strength of HSS drops below that of LSS with similar thicknesses beyond 600 ^{0}C.

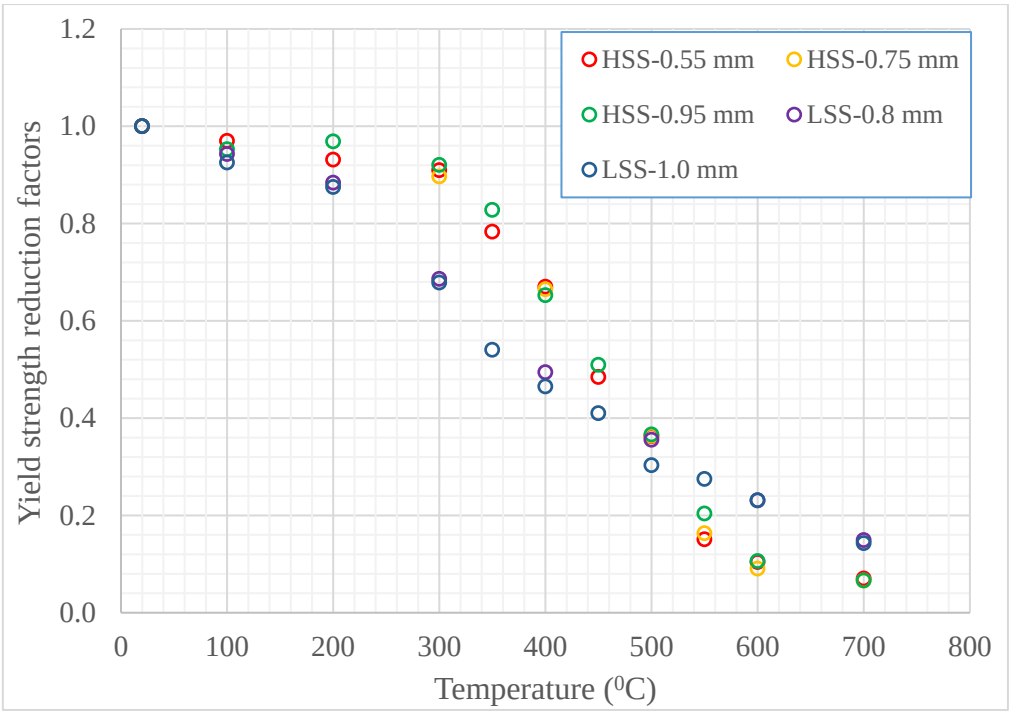

Fig. 7. Yield strength reduction factors of cold-rolled steel sheets

Table 1: Yield strengths of cold-rolled steel sheets at ambient and elevated temperatures in MPa

Temperature ^{0}C	High strength steel (G550)			Low strength steel (G300)	
	0.55 mm	0.75 mm	0.95 mm	0.8 mm	1.0 mm
20	706	668	618	349	318
100	685	-	589	329	295
200	658	-	599	309	279
300	642	599	569	240	216
350	553	-	512	-	172
400	473	444	404	173	148
450	342	-	315	-	131
500	256	243	227	124	97
550	107	109	126	-	88
600	74	61	66	81	74
700	50	44	41	52	46

3.3. Stress at 2% total strain

Eurocode 3 Part 1-2 [12] uses stress at 2% total strain as the yield strength at elevated temperatures for compact sections as higher strains are acceptable in an accidental limit state

such as fire [19]. Generally, the elevated temperature stress-strain curves of cold-formed steels exhibit a larger difference between the stress at 2% total strain and 0.2% proof stress compared to the corresponding difference in the ambient temperature stress-strain curve. Hence, Eurocode 3 Part 1-2 [12] utilises the capacity enhancement through strain hardening. However, Austrian standards such as AS/NZS 4600 [9] and AS 4100 [20] use 0.2% proof stress as the yield strength. Table 2 gives the stresses at 2% total strain of HSS and LSS at ambient and elevated temperatures.

The elevated temperature reduction factors for the stress at 2% total strain are higher than those of yield strength. They indicate that both LSS and HSS possess better strain hardening at elevated temperatures than at ambient temperature. Furthermore, there is no considerable reduction in the stress at 2% total strain of HSS up to 300 ^{0}C whereas there is a slight reduction for LSS. The reduction factors of stress at 2% total strain show similar behaviour as the yield strength reduction factors beyond 300 ^{0}C. However, the differences between the reduction factors of LSS and HSS are less than those of yield strength in the temperature range of 300 to 500 ^{0}C. It clearly shows that LSS exhibits higher strain hardening than HSS in that temperature range (Fig. 8).

Table 2: Stresses at 2% total strain of cold-rolled steel sheets at ambient and elevated temperatures in MPa

Temperature ^{0}C	High strength steel (G550)			Low strength steel (G300)	
	0.55 mm	0.75 mm	0.95 mm	0.8 mm	1.0 mm
20	706	668	622	352	320
100	685	-	608	340	299
200	677	-	621	330	292
300	697	650	625	312	295
350	611	-	564	-	244
400	528	489	449	231	200
450	394	-	341	-	165
500	306	289	267	151	118
550	136	128	156	-	107
600	93	79	85	91	86
700	54	47	48	55	49

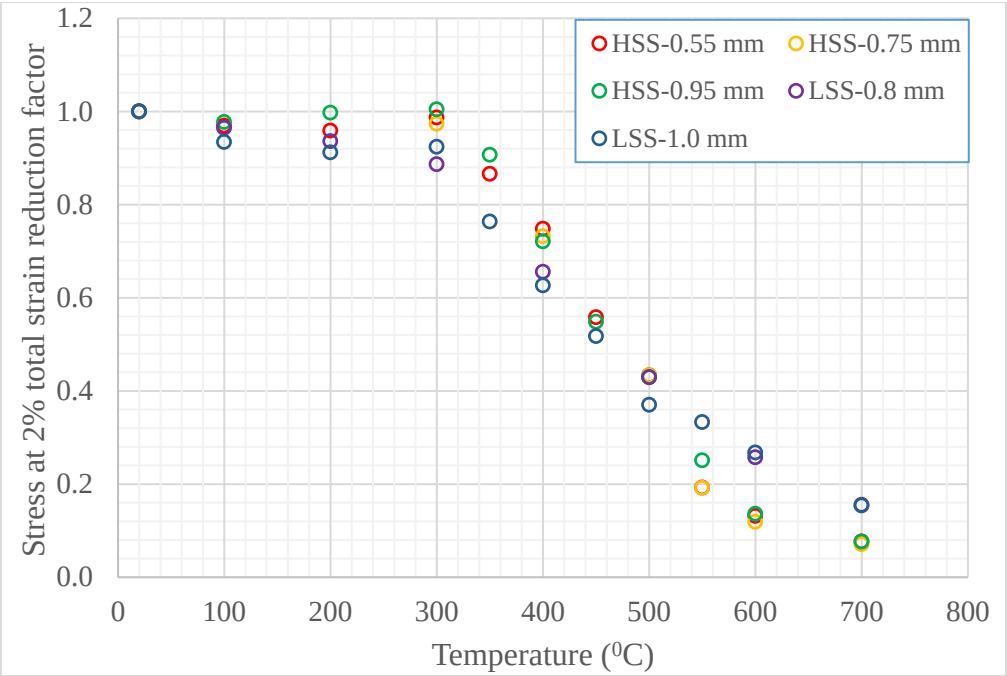

Fig. 8. Stress at 2% total strain reduction factors of cold-rolled steel sheets

3.4. 0.05% proof stress

Gardner and Yun [15] used a factor n (first strain hardening factor) to define the nonlinearity between proportional limit stress and yield strength of CFS at ambient temperature. This factor (n) is determined by using the ratio of yield strength to 0.05% proof stress. Hence it is useful to establish an elevated temperature reduction factor predictive equation for 0.05% proof stress.

Table 3 gives the 0.05% proof stresses of HSS and LSS at ambient and elevated temperatures. The difference between them and the yield strengths in Table 1 shows the level of nonlinearity of cold-rolled steel sheets. The 0.05% proof stress and yield strength of LSS and 0.55 mm HSS are the same at ambient temperature as they exhibit sharp yielding characteristics. However, 0.05% proof stress and yield strength of these cold-rolled steel sheets exhibit considerable differences at elevated temperatures, which indicate that they exhibit nonlinearity at elevated temperatures. The elevated temperature reduction factors of 0.05% proof stress show a similar reduction pattern as the yield strength reduction factors in Fig. 7.

Table 3: 0.05% proof stresses of cold-rolled steel sheets at ambient and elevated temperatures in MPa

Temperature ^{0}C	High strength steel (G550)			Low strength steel (G300)	
	0.55 mm	0.75 mm	0.95 mm	0.8 mm	1.0 mm
20	706	632	567	349	318
100	684	-	521	329	295
200	655	-	547	309	279
300	579	511	474	226	199
350	472	-	434	-	142
400	372	365	330	146	128
450	281	-	257	-	113
500	209	193	179	105	86
550	97	93	103	-	78
600	71	57	63	73	65
700	46	41	38	45	42

3.5. Proportional limit stress

Kankanamge and Mahendran [13] observed considerable nonlinearity in the stress-strain behaviour of cold-formed steels at elevated temperatures, and hence they defined the nonlinearity in terms of the ratio of proportional limit stress to yield strength. However, no reduction factors are given for the proportional limit stress of CFS in AS/NZS 4600 [9]. Eurocode 3 Part 1-2 [12] provides elevated temperature proportional limit stress to ambient temperature yield strength ratios. However, Kankanamge and Mahendran [2] and Imran et al. [5] have shown that the yield strength and Young's modulus reduction factors given in Eurocode 3 Part 1-2 [12] are not suitable for CFS. Similarly, the suitability of the proportional limit stress to ambient temperature yield strength ratios given in Eurocode 3 Part 1-2 [12] is questionable. Table 4 gives the proportional limit stresses from this study. They were determined as the stresses at which the linear stress-strain curves visibly change to nonlinear stress-strain curves. It is not possible to obtain accurate values of proportional limit stresses because experimental stress-strain curves do not show perfect linearity even within the linear portion of stress-strain curves.

Table 4: Proportional limit stresses of cold-rolled steel sheets at ambient and elevated temperatures in MPa

Temperature (^{0}C)	High strength steel (G550)			Low strength steel (G300)	
	0.55 mm	0.75 mm	0.95 mm	0.8 mm	1.0 mm
20	706	565	473	349	318
100	685	-	430	329	295
200	635	-	460	309	279
300	500	405	340	178	159
350	390	-	333	-	90
400	290	255	240	100	93
450	198	-	180	-	80
500	145	130	125	75	65
550	81	76	78	-	55
600	61	47	50	57	52
700	40	33	32	34	34

Similar to the 0.05% proof stress, the difference between yield strength and proportional limit stress also exhibits the level of nonlinearity. Proportional limit reduction factors of both HSS and LSS exhibit similar reduction pattern as the yield strength reduction factors in Fig. 7. However, the proportional limit stress reduction factor of LSS shows a large drop at 350 ^{0}C. This may be associated with the high level of strain hardening as reflected by the higher ultimate strength to yield strength ratio for LSS at 350 ^{0}C.

3.6. Young's modulus

It is very hard to determine the Young's modulus accurately at elevated temperatures as it is not possible to use strain gauges or clip type extensometers. The rod type extensometers provide reasonably accurate Young's modulus values. Imran et al. [5] examined the difference between the Young's modulus values at ambient temperature based on strain gauge and rod-type extensometer measurements and the maximum difference was 8% for flat coupons. The selection of the linear portion in the stress-strain curve is also a critical factor. Huang and Young [21] used the stress-strain curve up to 20-45% of the yield strength as linear for CFS. In this study the stress-strain curve up to 20-50% of the yield strength was used as the linear portion to determine the Young's modulus values given in Table 5 and Fig. 9. As seen in Fig. 9, HSS and LSS show almost similar elevated temperature reduction factors for Young's modulus.

Table 5: Young's modulus of cold-rolled steel sheets at ambient and elevated temperatures in MPa

Temperature ^{0}C	High strength steel (G550)			Low strength steel (G300)	
	0.55 mm	0.75 mm	0.95 mm	0.8 mm	1.0 mm
20	199014	204961	200245	189637	188292
100	183312	-	185930	171647	174360
200	167529	-	175256	166100	156359
300	159228	157105	158151	146579	135706
350	150395	-	141837	-	116730
400	136609	129871	138221	114194	108963
450	116744	-	105044	-	93342
500	96958	86477	91361	79440	81578
550	63479	68278	68730	-	64071
600	56627	54076	48546	56878	57688
700	36437	31787	26250	37000	28591

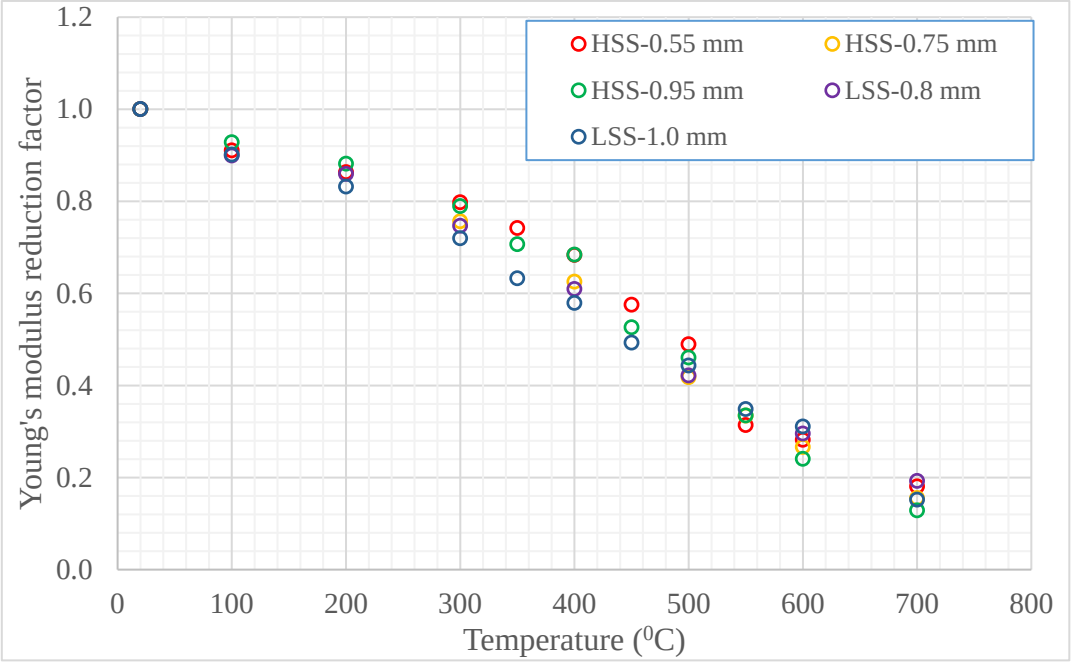

Fig. 9. Young's modulus reduction factors of cold-rolled steel sheets

3.7. Ultimate strength

The ultimate strength is the maximum stress in the stress-strain curve and is the end point of many theoretical stress-strain models. The difference between the yield and ultimate strengths

represents the level of strain hardening of steel. The ultimate strengths and the elevated temperature reduction factors are given in Table 6 and Fig. 10, respectively.

The ultimate strengths of both HSS and LSS at 200 ^{0}C and 300 ^{0}C are higher than the ambient temperature ultimate strengths. Kankanamge and Mahendran [2] and Imran et al. [5] also observed similar behaviour in their studies. Imran et al. [5] pointed out that this behaviour occurs due to the formation of Cottrell atmosphere, which leads to the serrations on the stress-strain curve (Portevin LeChatelier effect) in the temperature range of 200 – 300 ^{0}C. Moreover, the increment is higher for LSS. However, the ultimate strength reduces beyond 300 ^{0}C. Also, LSS and HSS show similar reduction factors up to 500 ^{0}C while LSS shows less reduction than HSS beyond 500 ^{0}C. Overall, the ultimate strength reduction factors of both HSS and LSS are higher than the yield strength reduction factors at a given temperature, and the difference is larger for LSS than HSS except at 600 ^{0}C and 700 ^{0}C as shown in Fig. 11. This shows that both LSS and HSS exhibit strain hardening behaviour at elevated temperatures and the level of strain hardening is higher for LSS than HSS except at 600 ^{0}C and 700 ^{0}C. As seen in Fig. 11, the ultimate strength of LSS is almost double the value of yield strength at 300 ^{0}C and 350 ^{0}C. Many design standards use yield strength to calculate the squash load even at elevated temperatures. Hence it raises a question whether the squash load is underestimated.

Table 6: Ultimate strengths of cold-rolled steel sheets at ambient and elevated temperatures in MPa

Temperature ^{0}C	High strength steel (G550)			Low strength steel (G300)	
	0.55 mm	0.75 mm	0.95 mm	0.8 mm	1.0 mm
20	710	668	628	389	371
100	692	-	614	381	351
200	712	-	667	476	440
300	709	654	632	458	415
350	614	-	568	-	338
400	529	489	449	301	257
450	395	-	357	-	199
500	307	292	268	183	140
550	148	143	164	-	126
600	108	92	101	104	97
700	57	51	51	57	51

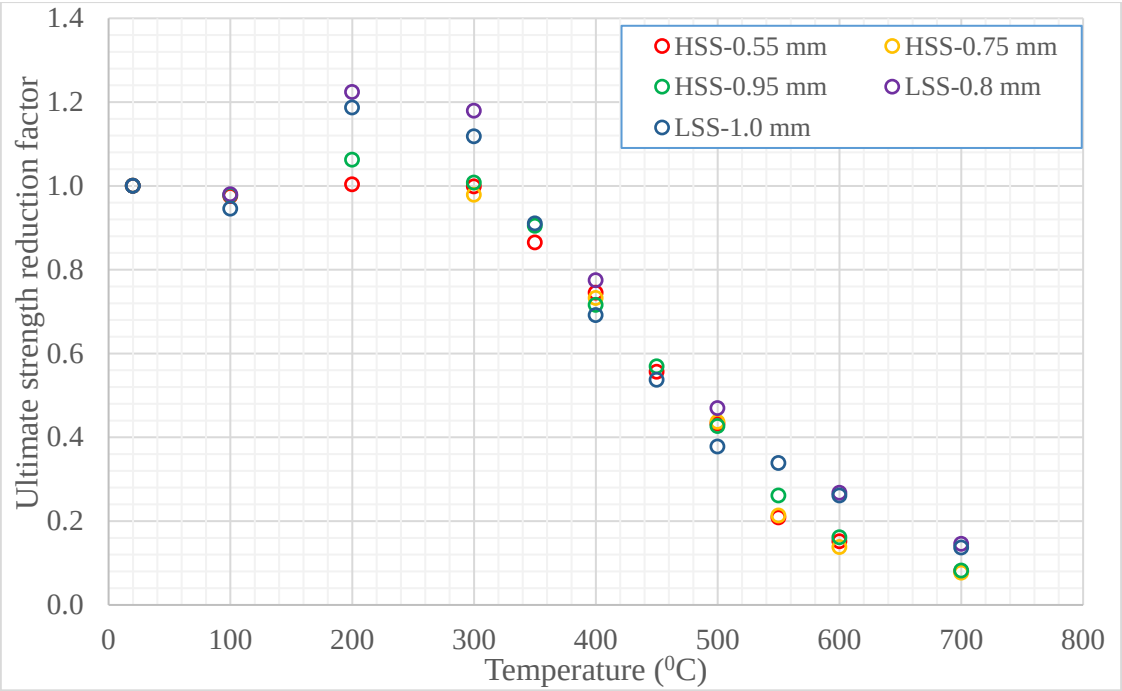

Fig. 10. Ultimate strength reduction factors of cold-rolled steel sheets

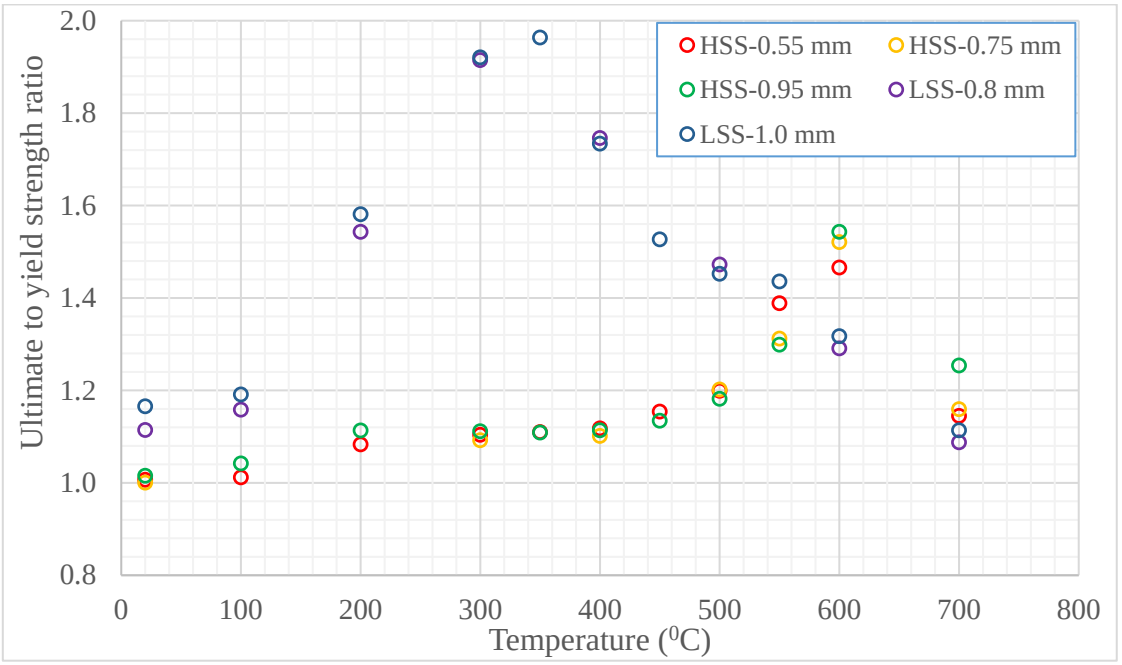

Fig. 11. Ultimate strength to yield strength ratio of cold-rolled steel sheets

3.8. Ultimate strain

The strains corresponding to the ultimate strengths, the ultimate strains, are shown in Fig. 12 as a function of temperature for HSS and LSS. The elevated temperature reduction factors of ultimate and yield strengths clearly show that CFS show a considerable level of strain hardening at elevated temperatures. Many researchers [22] have proposed a CSM to

incorporate the strain hardening of stainless steel and aluminium into their capacity predictions. In the CSM method, ultimate strain is one of the controlling parameters of design maximum strain, ε_{csm}. Moreover, ultimate strain is used to construct the two-stage model proposed by Gardner and Yun [15]. Hence it is necessary to determine the ultimate strains of CFS at elevated temperatures. The ultimate strains of 0.95 mm HSS between 400 and 500 ^{0}C and 0.75 mm HSS at 400 ^{0}C are slightly less than 2%. This raises questions about the suitability of using the stress at 2% total strain as yield strength at elevated temperatures as given in Eurocode 3 Part 1-2 [12].

As seen in Fig. 12, LSS show higher ultimate strains than HSS up to 550 ^{0}C. However, both steels show similar ultimate strains beyond 550 ^{0}C. The presence of almost similar ultimate strain, ultimate strength and yield strength values for HSS and LSS beyond 550 ^{0}C raises a question whether there is any difference among the cold-rolled steel grades beyond 550 ^{0}C.

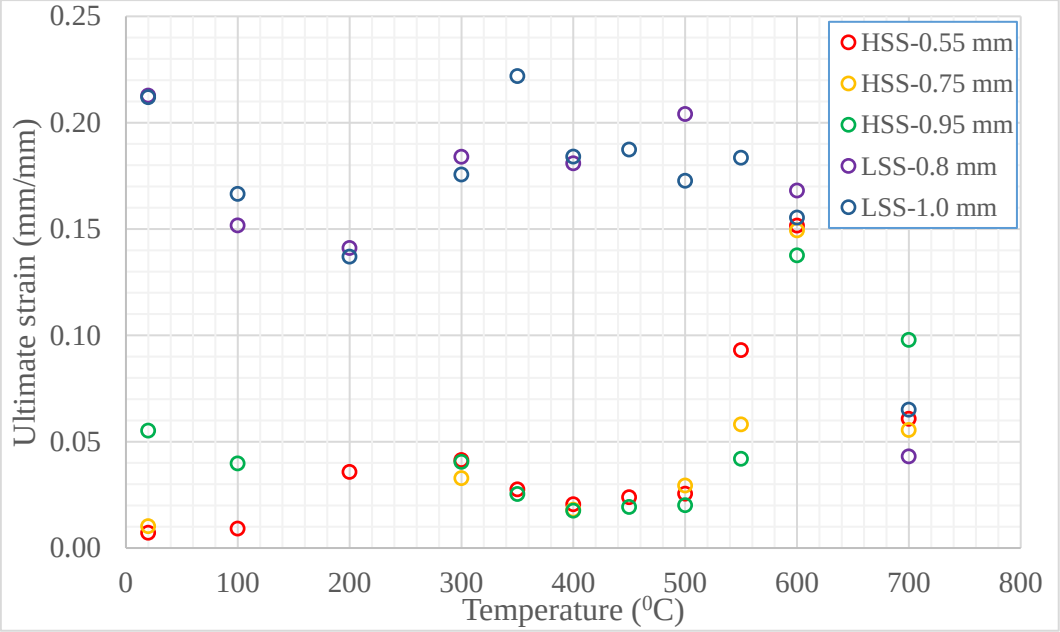

Fig. 12. Ultimate strain of cold-rolled steel sheets

3.9. Fracture strain

Fracture strain is one of the ductility parameters defined in AS/NZS 4600 [9] and Eurocode 3 Part 1-2 [12]. Although in general LSS exhibits higher ductility than HSS, the ductility of HSS rapidly increases beyond 550 ^{0}C. LSS and 0.95 mm HSS show reduction in ductility until they reach the lowest ductility at 200 ^{0}C where the ultimate strength is the highest and their ductility increases beyond 200 ^{0}C as the temperature rises. Fig. 13 shows the fracture strain versus temperature plot while Fig. 14 shows the fracture modes of tensile test coupons.

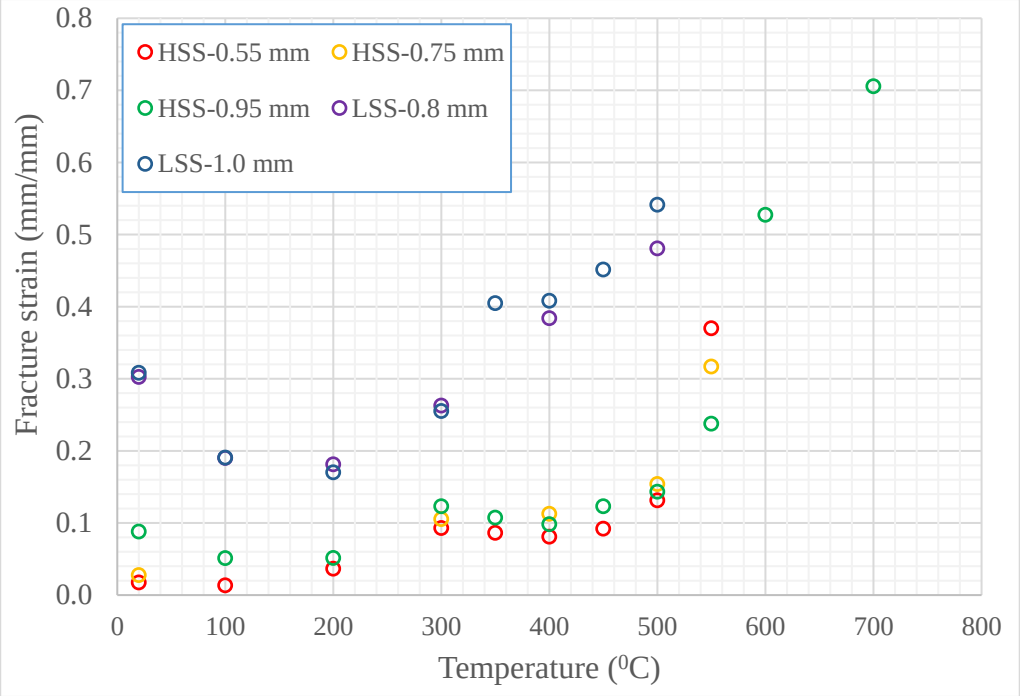

Fig. 13. Fracture strain of cold-rolled steel sheets

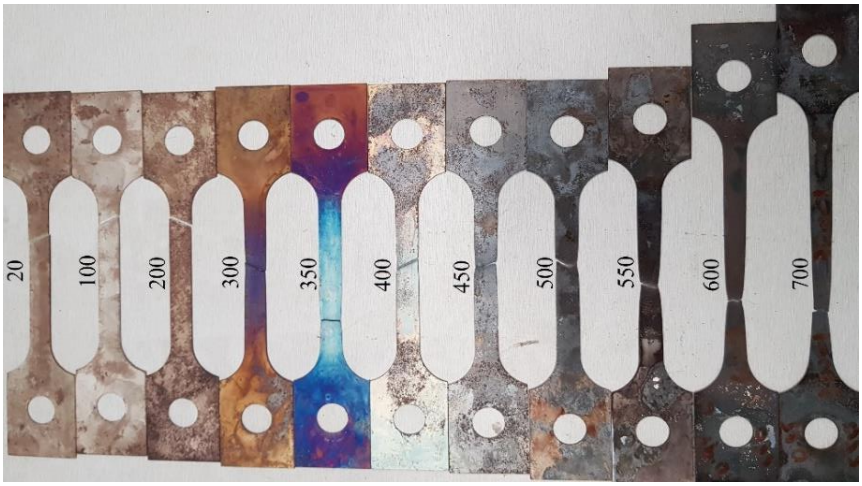

Fig. 14. Fracture modes of tensile test coupons (G550-0.95 mm)

4. Predictive equations

It is essential to summarise the experimental results in a usable format for designers and researchers to use them. Therefore, suitable predictive equations were developed to determine the elevated temperature mechanical properties with respect to ambient temperature mechanical properties. The predictive equations given in AS/NZS 4600 [9] for the reduction factors of yield strength and Young's modulus are based on Kankanamge and Mahendran's [2] experimental study, and they are compared with the experimental results of this study in Fig.

15. Since they exhibit a good agreement, the same predictive equations are recommended in this study. Such a good agreement demonstrates the accuracy and consistency of elevated temperature mechanical property test results. However, predictive equations are not available for the reduction factors of ultimate strength, stress at 2% total strain, 0.05% proof stress and proportional limit stress in Kankanamge and Mahendran [2], nor given in AS/NZS 4600 [9]. Therefore new predictive equations are proposed here. Also, the one-stage stress-strain model in AS/NZS 4600 [9] did not show good agreement with the experimental stress-strain curves of this study. Hence a two-stage stress-strain model is proposed to accurately predict the stress-strain behaviour of CFS based on the ambient temperature model of Gardner and Yun [15].

The mechanical property reduction factor predictive equations were developed first in this section based on the experimental results of cold-rolled steel sheets. The experimental results of cold-formed steel floor decks and lipped channels were then compared with the proposed equations. The proposed reduction factor equations are not simplified to a single equation covering all the temperatures. Instead different coefficients are given for different temperature ranges. Imran et al. [5] proposed a single equation for yield strength and Young's modulus reduction factors for all the temperatures as the reduction pattern suited a single equation. However, they did not propose a single equation for stress at 2% total strain and ultimate strength. On the other hand, Seif et al. [23] proposed a single equation for yield strength and Young's modulus of hot-rolled steels. However, the equations are complicated with many coefficients. A single equation is not possible for the reduction factors of cold-rolled steel sheets for all the temperatures as the reduction patterns do not suit a single equation. The use of single equations will reduce the accuracy of reduction factors. The equations will also be complicated with too many coefficients. Eurocode 3 Part 1-2 [12] gives reduction factors at temperatures in 100 ^{0}C intervals, instead of reduction factor equations.

The mechanical property predictive equations proposed in this section are based on elevated temperature tensile coupon test results of 52 HSS and 34 LSS along with ambient temperature tensile coupon test results of nine HSS and six LSS. Table 7 provides the details of the tension coupon tests. The yield strength and Young modulus reduction factor predictive equations given in AS/NZS 4600 [9] are based on the experimental results of Kankanamge and Mahendran [2], who tested 1.55 mm and 1.95 mm LSS (G250) and 1.5 mm and 1.9 mm HSS (G450) at 20, 100 to 700 ^{0}C (at 100 ^{0}C intervals). These test results were also used in deriving the reduction factor predictive equations of stress at 2% total strain and ultimate strength.

Hence, the predictive equations include most of the steel grades and thicknesses used to form CFS sections in the industry.

Table 7: Details of tension coupon tests

Steel Grade	Thickness (mm)	Test temperature (^{0}C)	Number of specimens
G550	0.55	20, 100, 200, 300, 350, 400, 450, 500, 550, 600, 700	23
	0.75	20, 300, 400, 500, 550, 600, 700	15
	0.95	20, 100, 200, 300, 350, 400, 450, 500, 550, 600, 700	23
G300	1.0	20, 100, 200, 300, 350, 400, 450, 500, 550, 600, 700	23
	0.8	20, 100, 200, 300, 400, 500, 600, 700	17

4.1. Yield strength and Young's modulus

AS/NZS 4600 [9] gives the elevated temperature yield strength and Young's modulus reduction factors using linear predictive equations in the format of $xT + y$, where T is temperature (^{0}C) and the two coefficients x and y are given in Table 8. However, a nonlinear equation of $25\ (1.16 - T^{0.022})$ is given for the elevated temperature yield strength reduction factors of LSS in the temperature range of 200 to 800 ^{0}C. AS/NZS 2327 [10] also gives the same elevated temperature yield strength and Young's modulus reduction factor equations given in AS/NZS 4600 [9] for HSS. The yield strength reduction factors depend on the steel grade while Young's modulus reduction factors do not depend on the steel grade as per the experimental results. Accordingly, AS/NZS 4600 [9] gives separate yield strength reduction factor predictive equations for LSS and HSS while it gives the same Young's modulus reduction factor predictive equation for LSS and HSS.

Table 8: Elevated temperature reduction factor equations and coefficients for yield strength and Young's modulus in AS/NZS 4600 [9]

Mechanical property	Steel type	Temperature range (^{0}C)	x	y
Yield strength	HSS	0 - 300	-0.000179	1.00358
		300 - 600	-0.0028	1.79
		600 - 800	-0.0004	0.35
	LSS	0 - 200	-0.0005	1.01
		200 - 800	$25\ (1.16 - T^{0.022})$	
Young's modulus	HSS or LSS	0 - 200	-0.000835	1.0167
		200 - 600	-0.00135	1.1201

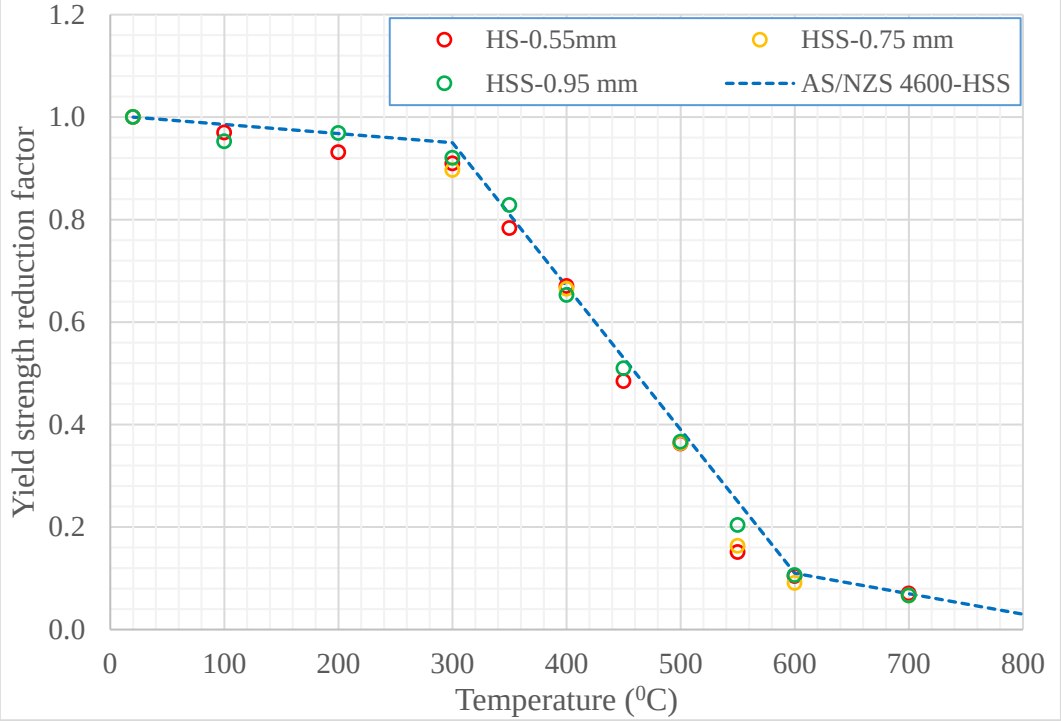

a. Yield strength reduction factors – HSS

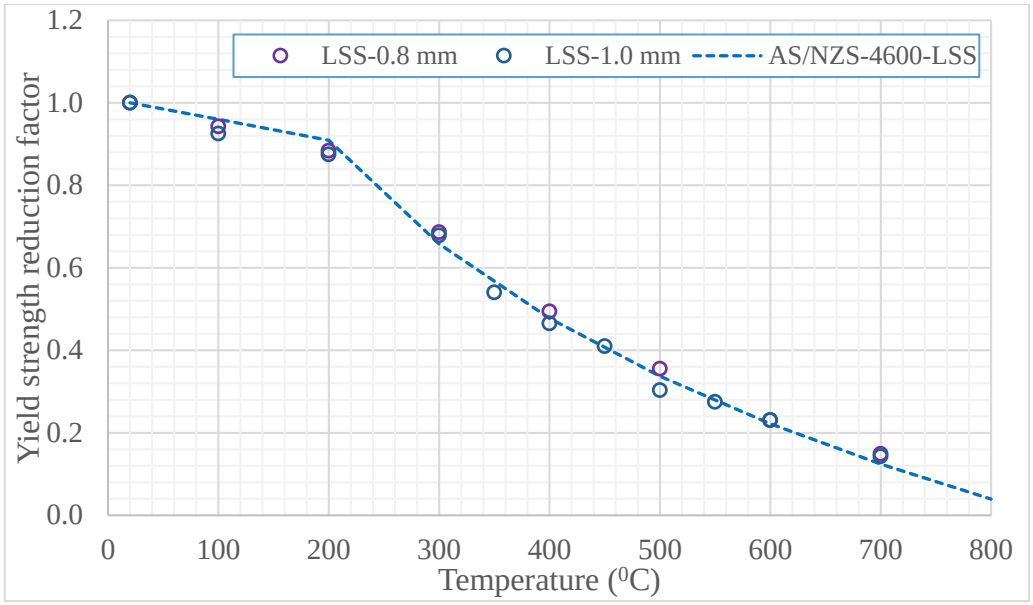

b. Yield strength reduction factors – LSS

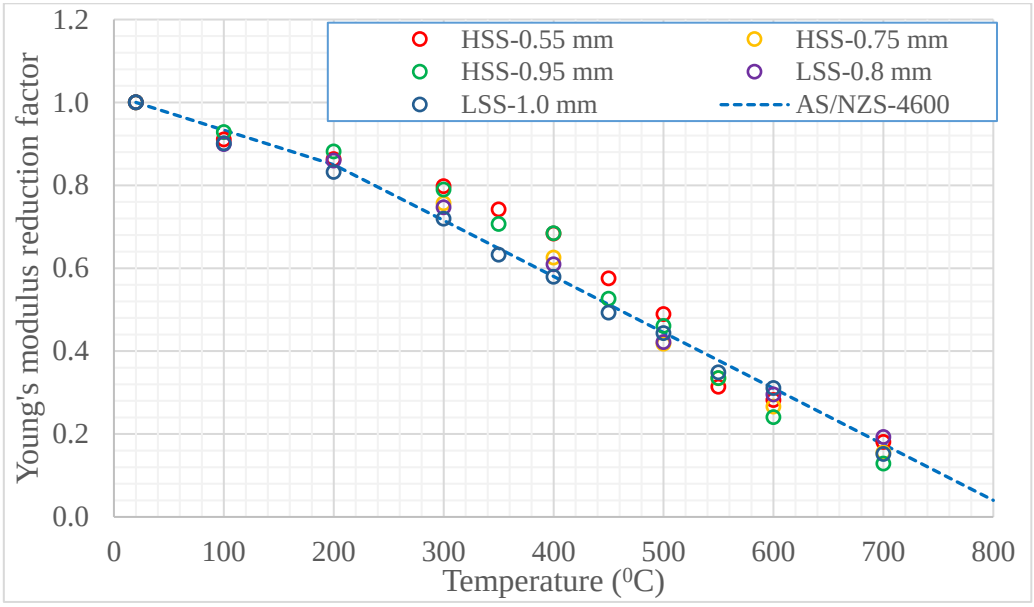

c. Young's modulus reduction factors

Fig. 15. Comparison of experimental results with AS/NZS 4600 [9] predictive equations for yield strength and Young's modulus reduction factors

4.2. Ultimate strength, stress at 2% total strain, 0.05% proof stress and proportional limit stress

These stress parameters are essential to formulate a two-stage stress-strain model and to study the effects of strain hardening and nonlinearity on the capacity of CFS structural elements at elevated temperatures. However, suitable predictive equations are not given in AS/NZS 4600

[9] for their reduction factors at elevated temperatures. Therefore, new predictive equations are proposed in the form of Equation 1.

$$f_T/f_{20} = 1/(x + y\ e^{\frac{T}{z}}) \qquad 20\ ^0C \le T \le 700\ ^0C \tag{1}$$

where, T is temperature, x, y and z are coefficients, f_T and f_{20} are stresses at elevated temperature T and ambient temperature, respectively.

Table 9: Coefficients x, y and z to determine the elevated temperature reduction factors for ultimate strength, stress at 2% total strain, 0.05% proof stress and proportional limit stress

Stress type	Steel type	Temperature range (^{0}C)	x	y	z
Ultimate strength	HSS	0 – 200	1.005	-0.0041	74
		200 - 600	0.899	0.0041	84
		600 - 700	3.10		91
	LSS	0 – 200	1.03	-0.024	94
		200 - 700	0.701	0.024	120
Stress at 2% total strain	HSS	0 – 300	1	0	1
		300 - 600	0.86	0.0033	80
		600 - 700	3.82		88
	LSS	0 – 300	0.957	0.039	216
		300 - 700	0.76		136
0.05% proof stress	HSS	0 – 600	0.994	0.005	81
		600 - 700	6.30		94
	LSS	0 – 200	0.681	0.305	444
		200 - 700	0.38		213
Proportional limit stress	HSS	0 – 600	0.994	0.014	91
		600 - 700	7.90	0.005	92
	LSS	0 – 200	0.681	0.305	453
		200 - 350	0.94	0.009	63
		350 - 700	0.70	0.80	300

Kankanamge and Mahendran's [2] experimental results (shown as KM in Fig. 16) were also used in deriving the predictive equations for the reduction factors of ultimate strength and stress at 2% total strain. However, the predictive equations for the reduction factors of 0.05% proof stress and proportional limit stress were derived using only the experimental results of this study as 0.05% proof stresses and proportional limit stresses are not reported in [2]. Figs. 16 to

19 exhibit a good comparison between the proposed equation and experimental results and thus confirm the suitability of using Equation 1 with its associated coefficients x, y and z given in Table 9 in predicting the elevated temperature reduction factors for ultimate strength, stress at 2% total strain, 0.05% proof stress and proportional limit stress.

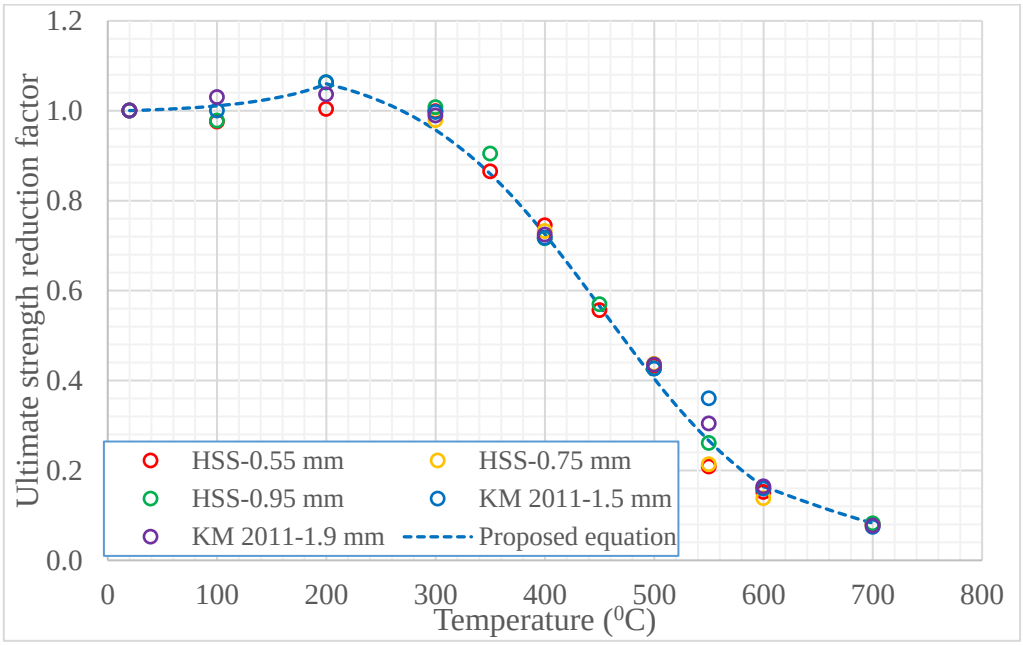

a. HSS

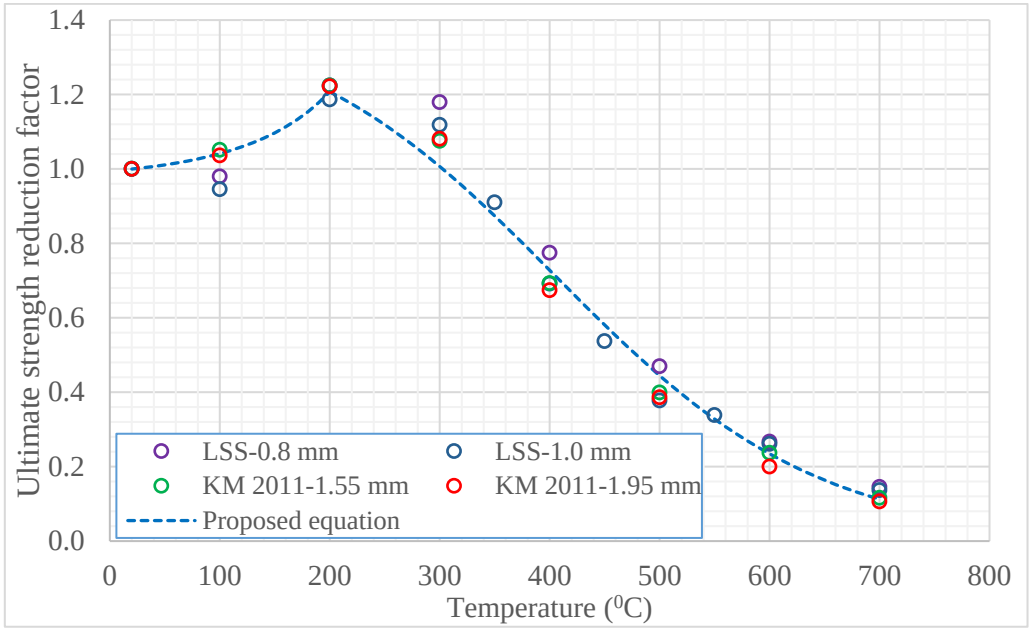

b. LSS

Fig. 16. Comparison of the proposed equation for the ultimate strength reduction factor with experimental results

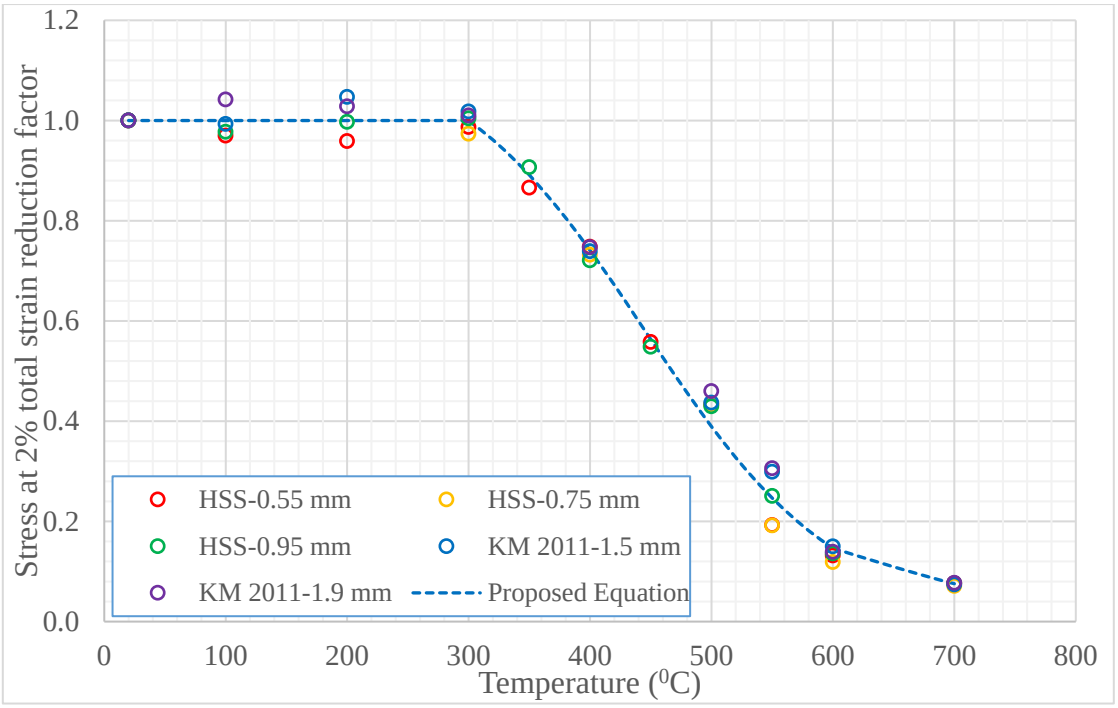

a. HSS

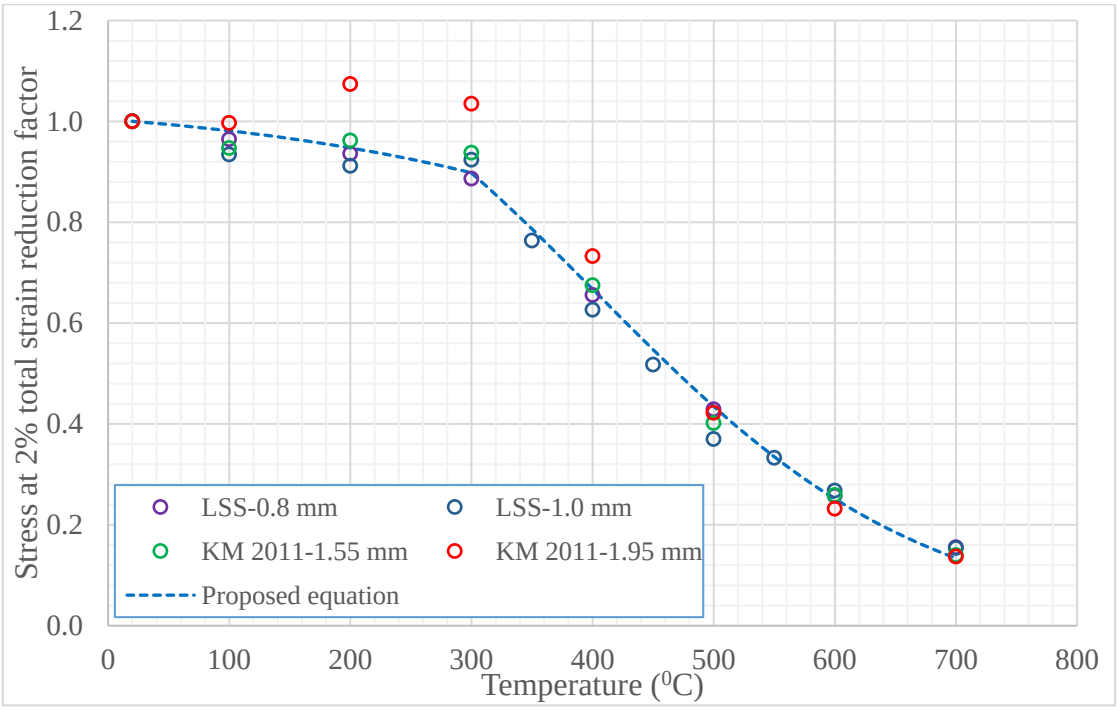

b. LSS

Fig. 17. Comparison of the proposed equation for the stress at 2% total strain reduction factor with experimental results

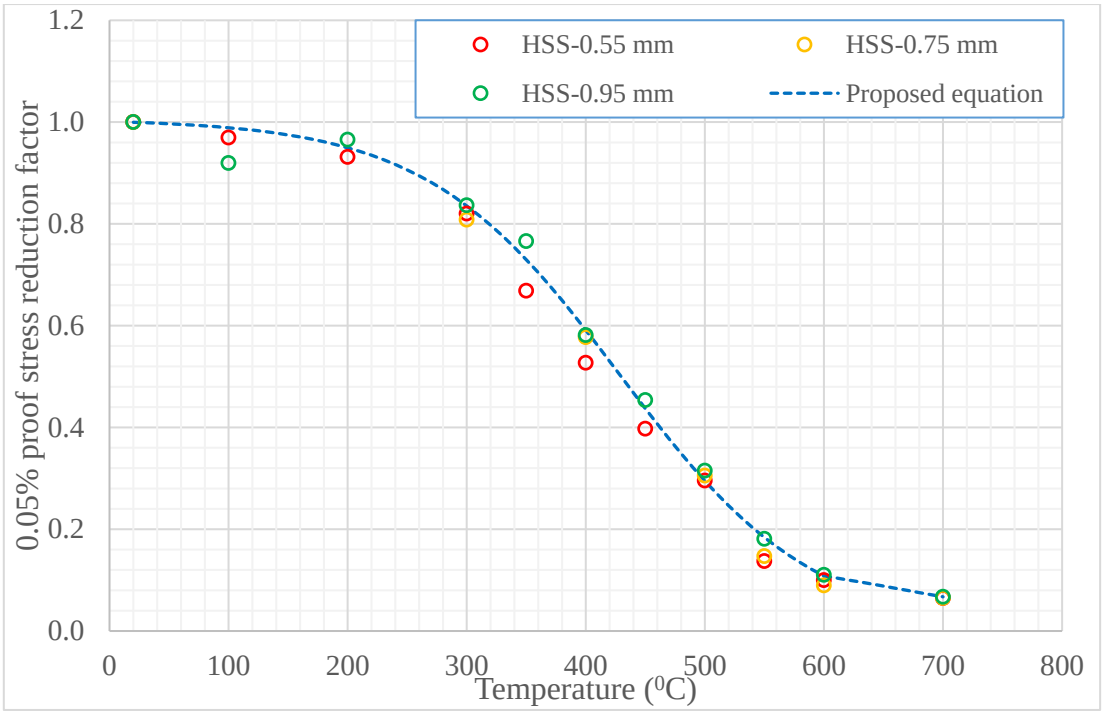

a. HSS

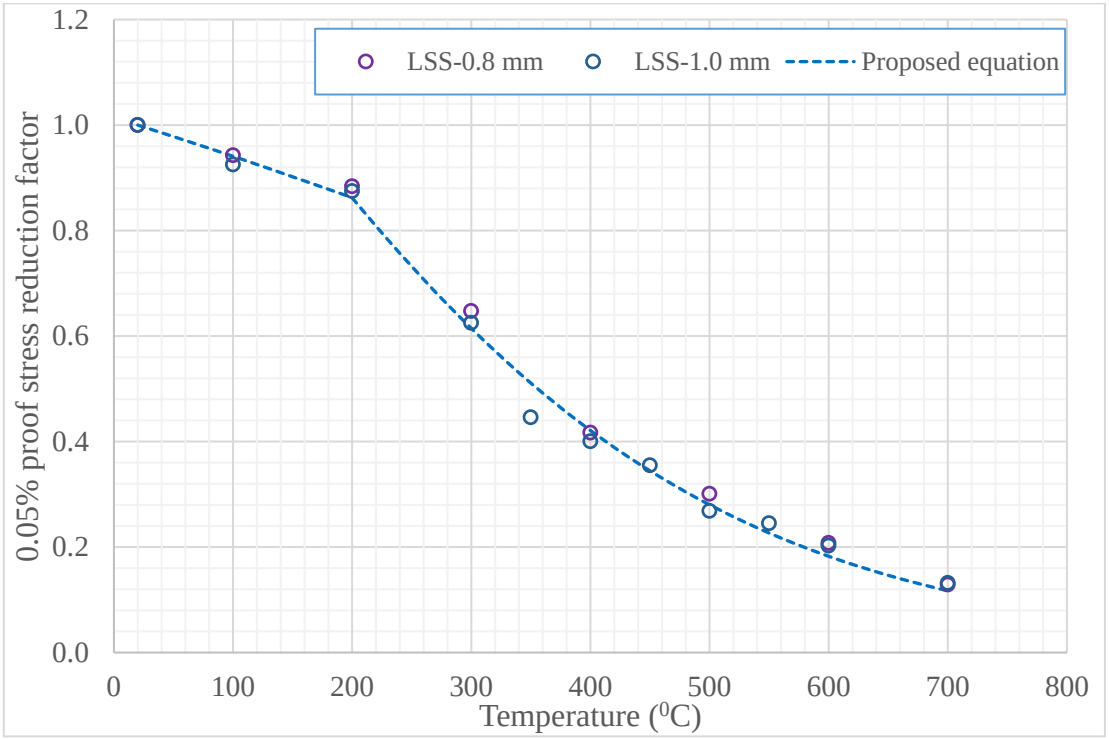

b. LSS

Fig. 18. Comparison of the proposed equation for the 0.05% proof stress reduction factor with experimental result

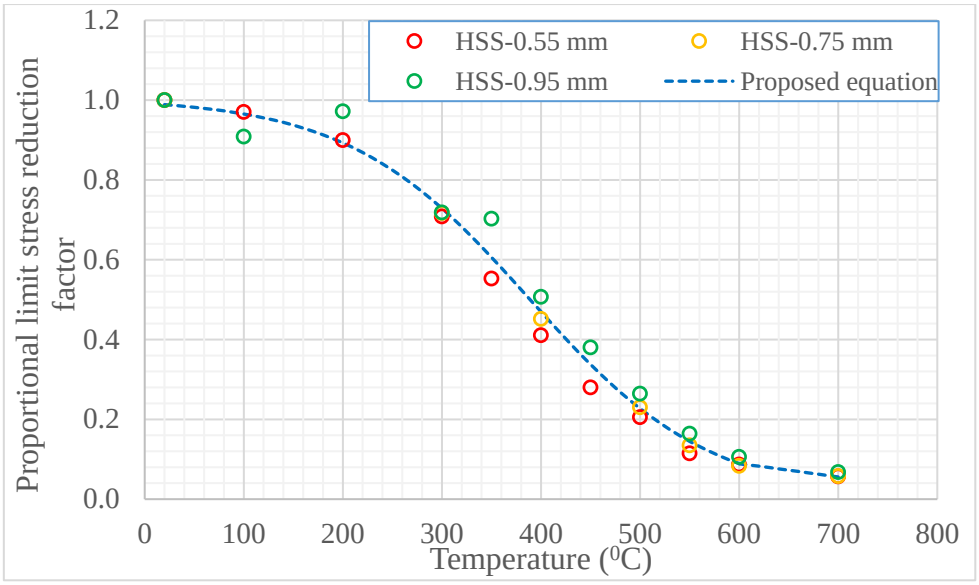

a. HSS

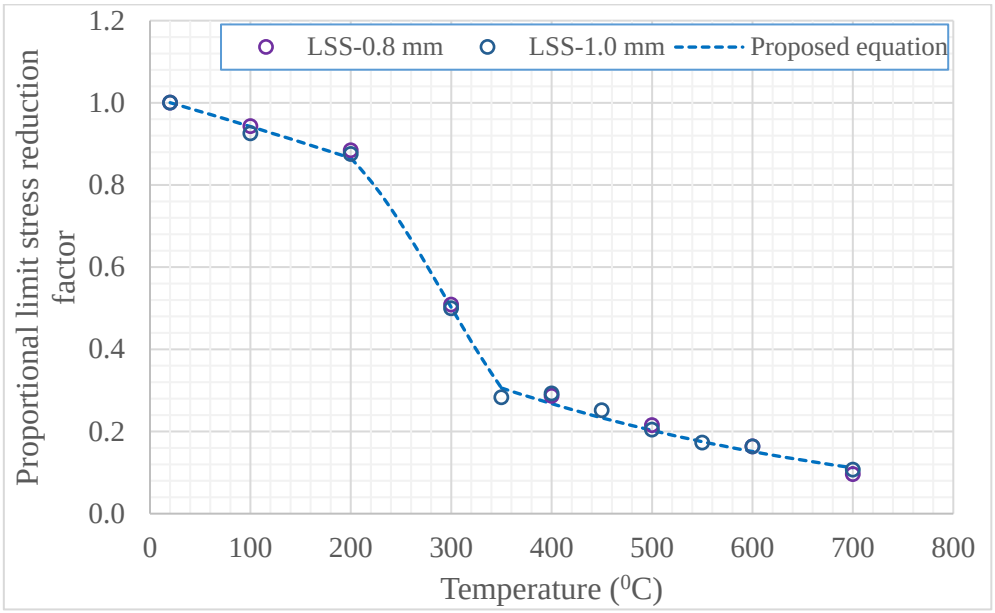

b. LSS

Fig. 19. Comparison of the proposed equation for the proportional limit stress reduction factor with experimental result

4.3. Ultimate strain

It is not practical to provide a predictive equation for the ultimate strain of cold-rolled steel sheets at elevated temperatures with reference to their ambient temperature ultimate strain as its ultimate strain shows a staggered variation with temperature. Gardner and Yun [15] proposed a relationship between ultimate strains and yield strength to ultimate strength ratios

at ambient temperature. However, the ultimate strain versus yield strength to ultimate strength ratio curve does not show a relationship at elevated temperatures (Fig. 20). Approximate values of ultimate strain at a given elevated temperature can be read from the graphs in Fig. 21, which is based on the average values of ultimate strain obtained from the experiments.

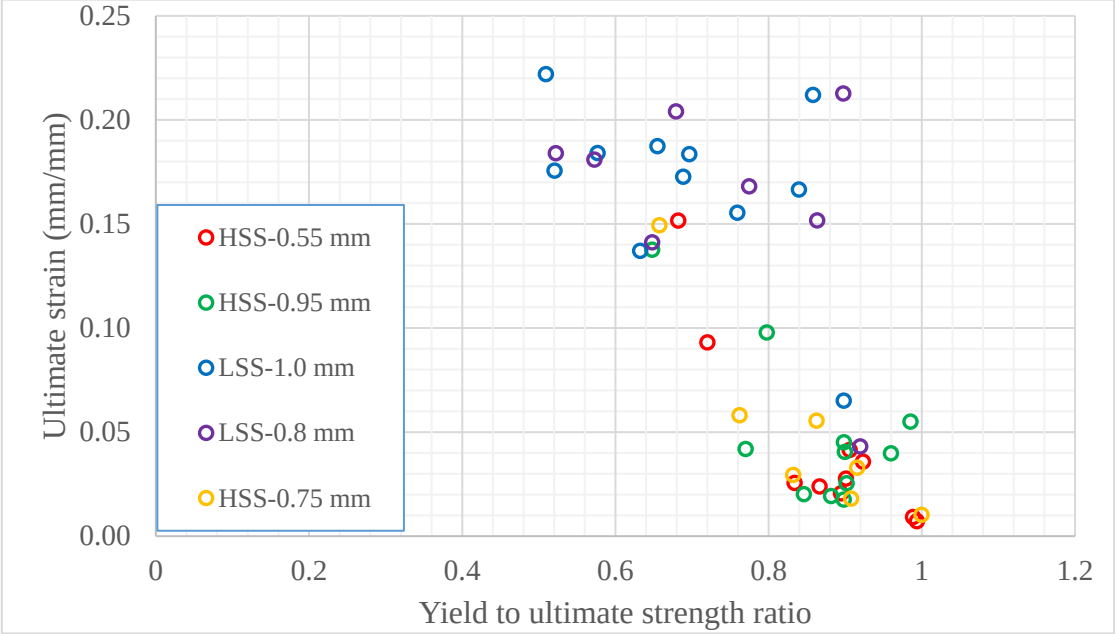

Fig. 20. Ultimate strain versus yield strength to ultimate strength ratio

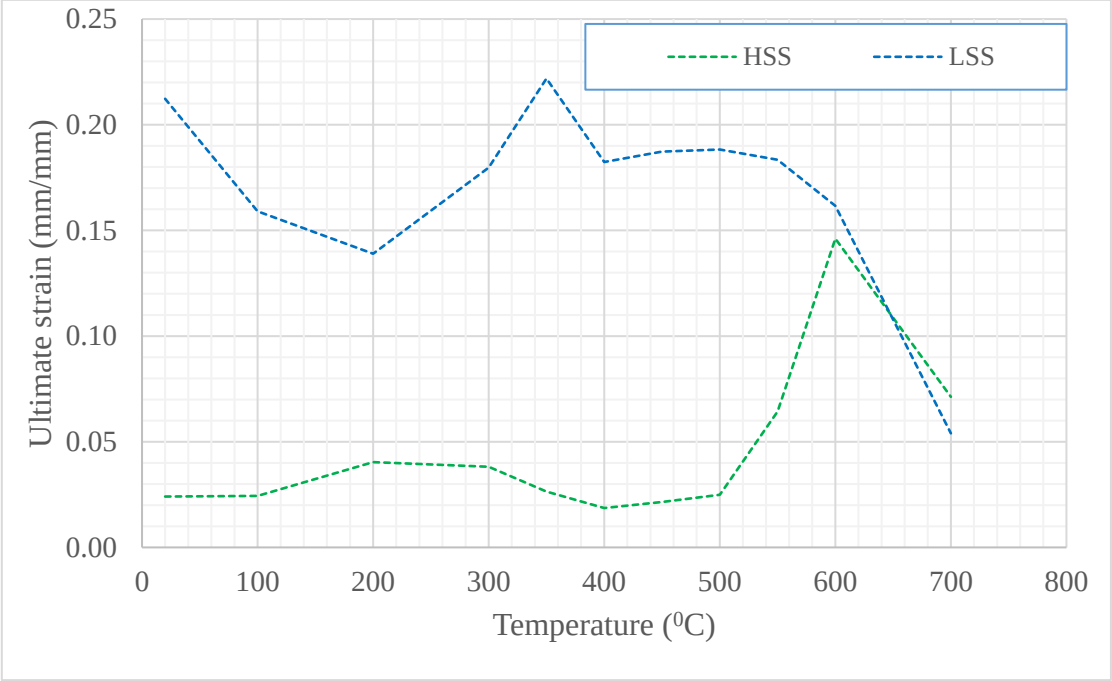

Fig. 21. Average ultimate strain of cold-rolled steel sheets at elevated temperatures

4.4. Stress-strain curve

The stress-strain curve of CFS is rarely used in design standards as the capacity predictive equations use only the key mechanical properties such as yield strength and Young's modulus of CFS. However, its use is increasing, especially in fire safety engineering as the industry is moving towards performance based solutions based on advanced numerical analyses. It is also needed for research purposes, and thus emphasising the need for accurate stress-strain curves.

The stress-strain model given in AS/NZS 4600 [9] predicts the stress-strain curves of low strength CFS accurately, but not for 300 ^{0}C (Fig. 22(b)). For 300 ^{0}C, it shows a high level of nonlinearity than experimental stress-strain curve. In contrast, it shows a low level of nonlinearity and strain hardening than the experimental stress-strain curves for high strength CFS and does not agree well for HSS at any elevated temperature (Fig. 22(a)). Importantly, the one-stage stress-strain model in AS/NZS 4600 [9] does not depend on either ultimate strain or ultimate strength. This is the main reason for these differences. Therefore it is necessary to formulate a simplified multi-stage model or a two-stage model for a more accurate prediction of the elevated temperature stress-strain curves of CFS. It is not practical to provide two separate stress-strain models, ie. one for LSS at temperatures higher than 350 ^{0}C (AS/NZS 4600 [9] stress-strain model) and another one for HSS at all temperatures and LSS at 300 ^{0}C (two-stage or multi-stage stress-strain model). Also, HSS is more commonly used in CFS construction than LSS. Hence, a suitable stress-strain model suitable for both HSS and LSS is needed. Details of the one-stage stress-strain model of AS/NZS 4600 [9] are given next.

$$\varepsilon_T = \frac{f_T}{E_T} + \beta\left[\frac{f_{y,T}}{E_T}\right]\left[\frac{f_T}{f_{y,T}}\right]^{\eta_T} \quad (2)$$

where

$\varepsilon_T =$ strain corresponding to given stress f_T at temperature (T)

E_T and $f_{y,T}$ = Young's modulus and yield strength at temperature (T), respectively, and

η_T and β are two parameters

For high strength steels $20^0C \leq T \leq 800^0C$

$$\beta = 0.86 \text{ and } \eta_T = -3.05 \text{ x } 10^{-7}T^3 + 0.0005\,T^2 - 0.2615T + 62.653 \quad (3)$$

For low strength steels $300^0C \leq T \leq 800^0C$

$$\beta = 1.5 \text{ and } \eta_T = 0.000138\,T^2 - 0.085468T + 19.212 \quad (4)$$

For low strength steels at $T < 300^0C$, elastic perfect plastic material model is used.

Wang et al. [24] proposed a multi-stage stress-strain model for HSS Bisalloy 80. The first stage is from zero to the proportional limit stress while the second stage is between the proportional limit stress and yield strength. The third and fourth stages cover strain hardening and softening processes, respectively. Eurocode 3 Part 1-2 [12] also gives a similar multi-stage stress-strain model for carbon steels at elevated temperatures.

Holmquist and Nadai [25] proposed a two-stage stress-strain model first with the first stage from zero to the proportional limit stress and the second stage for stresses beyond the proportional limit stress. Their model was later simplified by Ramberg and Osgood [14] with a close approximation as a one-stage stress-strain model. Ramberg and Osgood's [14] model theoretically gives zero proportional limit stress due to the strain term of $0.002\left[\frac{f}{f_y}\right]^n$ added to the linear elastic model $\left(\frac{f}{E}\right)$. Hence, the theoretical accuracy of Ramberg and Osgood's [14] model is questionable for materials with non-zero proportional limit stress. However, Mirambell and Real [26], Macdonald et al. [27] and Rasmussen [28] did not change Ramberg and Osgood's [14] model between zero stress and yield strength although they modified the Ramberg and Osgood's [14] one-stage model into a two-stage model (first stage between zero stress and yield strength and the second stage between yield and ultimate strengths), highlighting that Ramberg and Osgood's [14] predictions between yield and ultimate strengths are not accurate. Also, the developed two-stage stress-strain model was validated using experimental results. Similarly, Gardner and Yun [15] also adopted the simplification made by Ramberg and Osgood [14] in their two-stage stress-strain model for cold-formed steels at ambient temperature. Eurocode 3 Part 1-2 [12] also gives a similar two-stage stress-strain model for stainless steels at elevated temperatures. The multi-stage stress-strain models are more complex than the two-stage stress-strain models.

The accuracy of the first and second stages of a four-stage stress-strain model depends on the proportional limit stress. However, it is difficult to obtain the proportional limit stress accurately from the experimental stress-strain curves. Stang and Whittemore [29] defined the proportional limit stress as the stress at which the measured strain exceeded the strain calculated from linear elastic model by 12 μ (x10 $^{-6}$) while Wang et al. [24] selected 7 μ (x10 $^{-}$

^{6}) instead of 12 μ (x10 $^{-6}$). Wang et al. [24] proposed an average value of 0.65 for the proportional limit stress to yield strength ratio to avoid the difficulties in finding the proportional limit stress. This approximation may reduce the accuracy of the four-stage stress-strain model.

Eurocode 3 Part 1-2 [12] stress-strain model for carbon steel has the shortcoming of using the proportional limit stress as one of the parameters. It gives yield strain as 0.02 because it uses the stress at 2% total strain as yield strength. Also, it uses 0.2 as the ultimate strain without a strain hardening part regardless of the temperature. Although it permits the use of strain hardening part for advanced analysis, it is limited to 400 ^{0}C. Eurocode 3 Part 1-2 [12] stress-strain model and associated parameters are based on the experimental results of hot-rolled steels and is not suitable for CFS. This may be the reason why a separate stress-strain model is given for stainless-steel whose stress-strain behaviour is similar to that of CFS. Experimental stress-strain curves of HSS and LSS (Figs. 5 and 6) do not agree well with Eurocode 3 Part 1.2 stress-strain model for carbon steels and thus it was not considered in this paper

Wang et al. [24] included the softening portion of stress-strain curves in their theoretical stress-strain models. However, Eurocode 3 Part 1-2 [12] includes a linear softening portion with zero fracture stress to avoid complexity [30]. Softening portions of stress-strain curves are used for fracture modelling. However, the chance of CFS members subject to fracture is less at elevated temperatures than ambient temperature due to their increased ductility at elevated temperatures. Also, Garlock and Selamet [30], who studied the modelling and behaviour of steel plate connections subject to various fire scenarios, did not use the softening portion. Instead they assumed that the model failed when 20% total strain was reached. CFS exhibits higher differences between ultimate and fracture strains at elevated temperatures. Therefore, the theoretical stress-strain model will be more complex for the softening portion. Also, the fracture strains given in this study (Fig. 13) can be used for a linear softening model similar to that in Eurocode 3 Part 1-2 [12] if researchers are interested in using a softening portion in fracture modelling.

Despite the availability of several stress-strain models, it is essential to determine an optimum solution between accurate prediction and simplified model. Hence, the following two-stage stress-strain model is proposed for CFS at elevated temperatures based on the ambient temperature stress-strain model proposed by Gardner and Yun [15].

$$\varepsilon_T = \frac{f_T}{E_T} + 0.002\left[\frac{f_T}{f_{y,T}}\right]^n \quad \text{for } f_T < f_{y,T} \tag{5}$$

$$\varepsilon_T = \frac{f_T - f_{y,T}}{E_{0.2}} + \left[\varepsilon_{u,T} - \varepsilon_{0.2,T} - \frac{f_{u,T} - f_{y,T}}{E_{0.2}}\right]\left[\frac{f_T - f_{y,T}}{f_{u,T} - f_{y,T}}\right]^m + \varepsilon_{0.2,T} \quad \text{for } f_{y,T} \le f_T \le f_{u,T} \text{ and } \varepsilon_T \le \varepsilon_{u,T} \tag{6}$$

where

$\varepsilon_T =$ strain corresponding to given stress f_T at temperature (T)

$E_T, f_{y,T}, f_{u,T} =$ Young's modulus, yield strength and ultimate strength at temperature (T), respectively

$\varepsilon_{0.2,T}, \varepsilon_{u,T}, =$ yield strain and ultimate strain at temperature (T), respectively

The nonlinearity factor n is determined from

$$n = \frac{\ln(4)}{\ln(f_{y,T}/f_{0.05,T})} \tag{7}$$

where, $f_{0.05,T}$ is 0.05% proof stress at temperature (T).

The strain hardening factor m is determined from

For high strength steels $m = 1 + {3.3\, f_{Y,T}}/{f_{u,T}}$ $20\ ^0C \le T \le 700\ ^0C$ (8)

For low strength steels $m = 1 + {4.3\, f_{Y,T}}/{f_{u,T}}$ $20\ ^0C \le T \le 700\ ^0C$ (9)

The tangent modulus of the stress-strain curve at the yield point $E_{0.2}$ is determined from

$$E_{0.2} = \frac{E_T}{1 + 0.002\, n \frac{E_T}{f_{y,T}}} \tag{10}$$

Fig. 23 compares the stress-strain curves predicted by the proposed two-stage stress-strain model with experimental stress-strain curves. It shows a good agreement for both low and high strength CFS. However, the calculation process involves many parameters in deriving the stress-strain curve and is more complicated than that for the one-stage stress-strain model of AS/NZS 4600 [9], but less complicated than the multi-stage models.

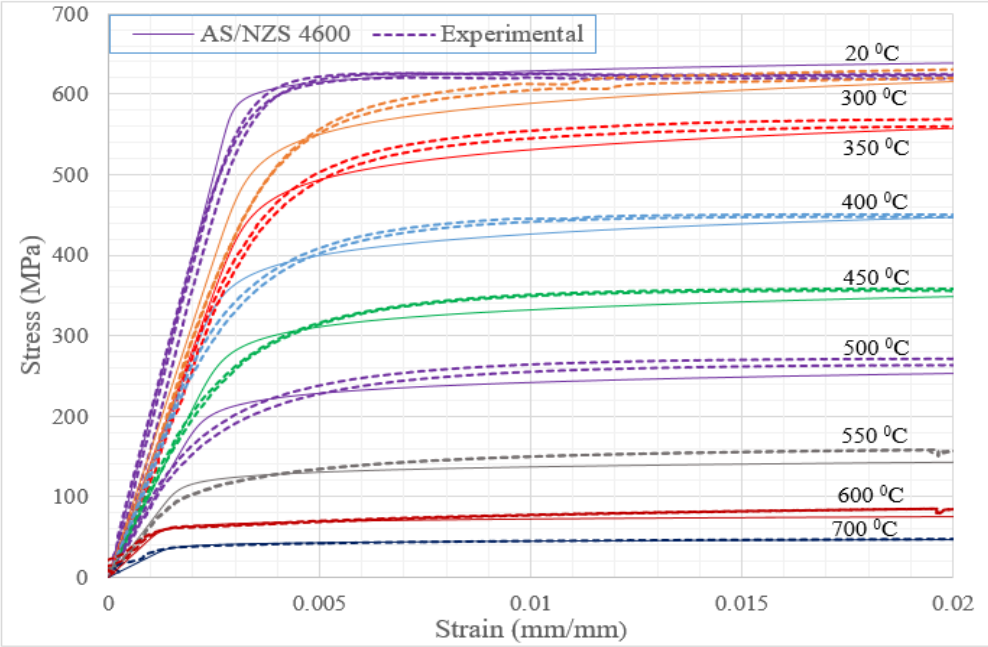

a. G550-0.95 mm cold-rolled steel sheet

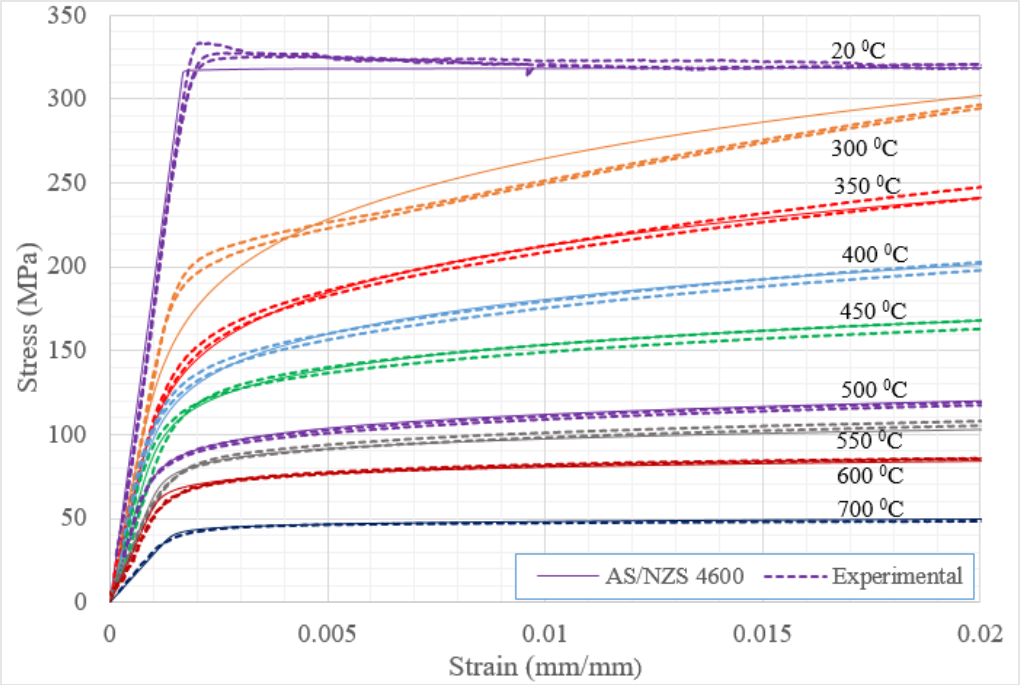

b. G300-1.0 mm cold-rolled steel sheet

Fig. 22. Comparison of stress-strain curves predicted by the one-stage model in AS/NZS 4600 [9] with experimental stress-strain curves

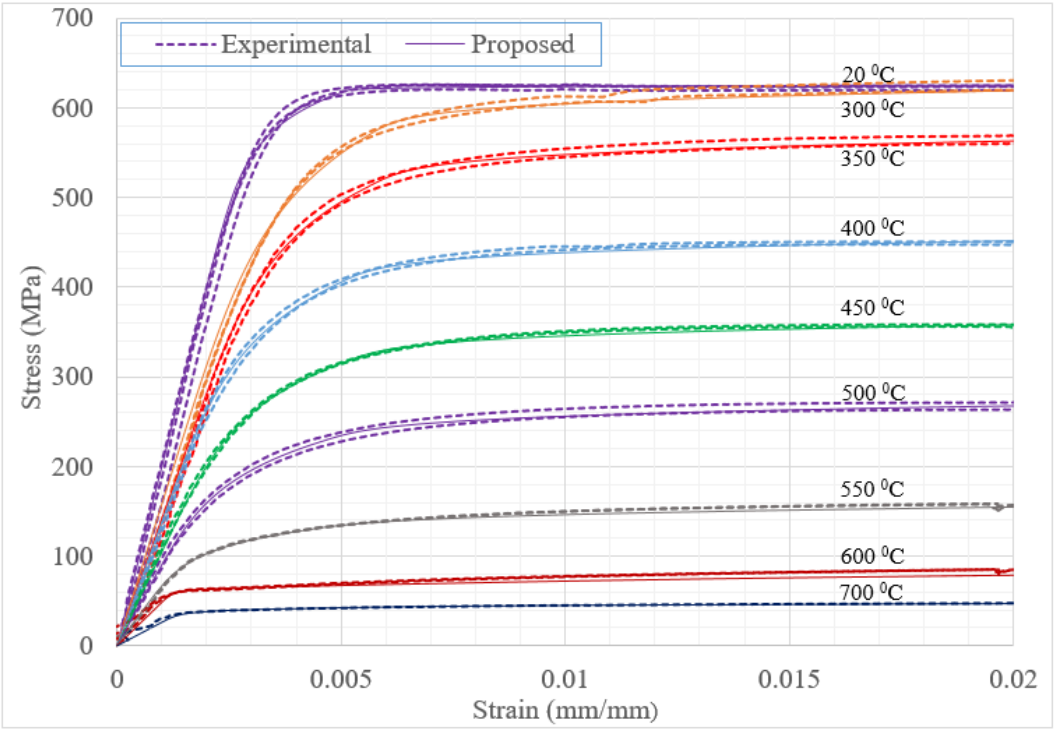

a. G550-0.95 mm cold-rolled steel sheet

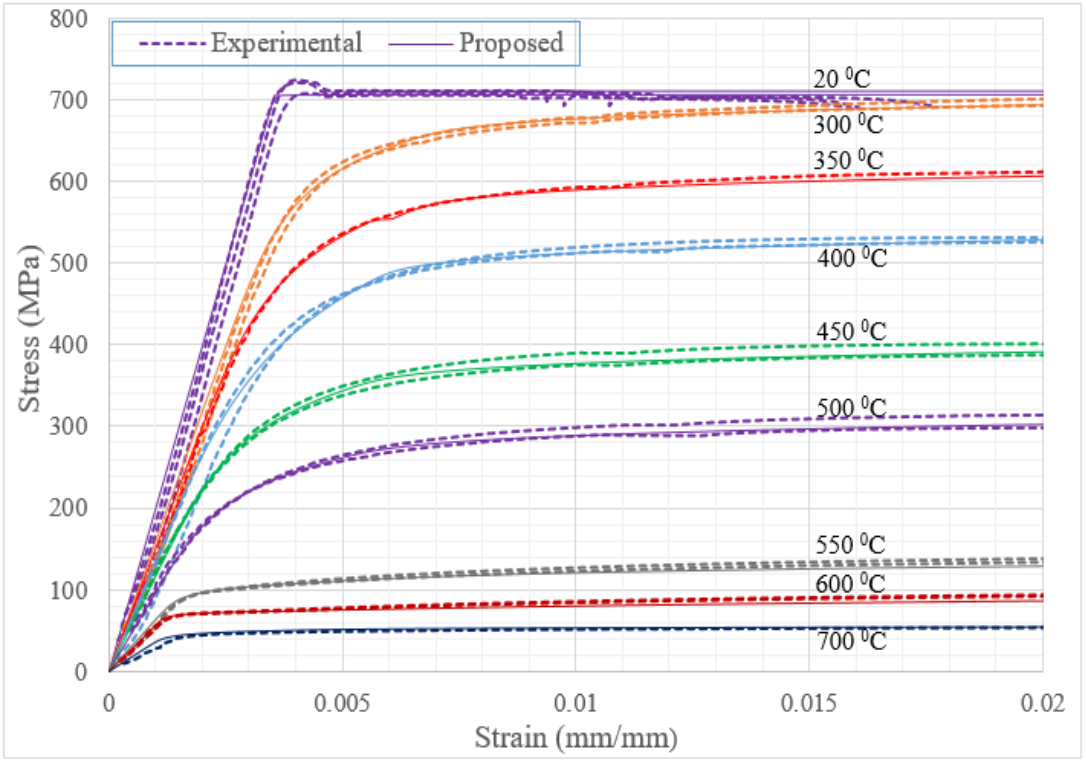

b. G550-0.55 mm cold-rolled steel sheet

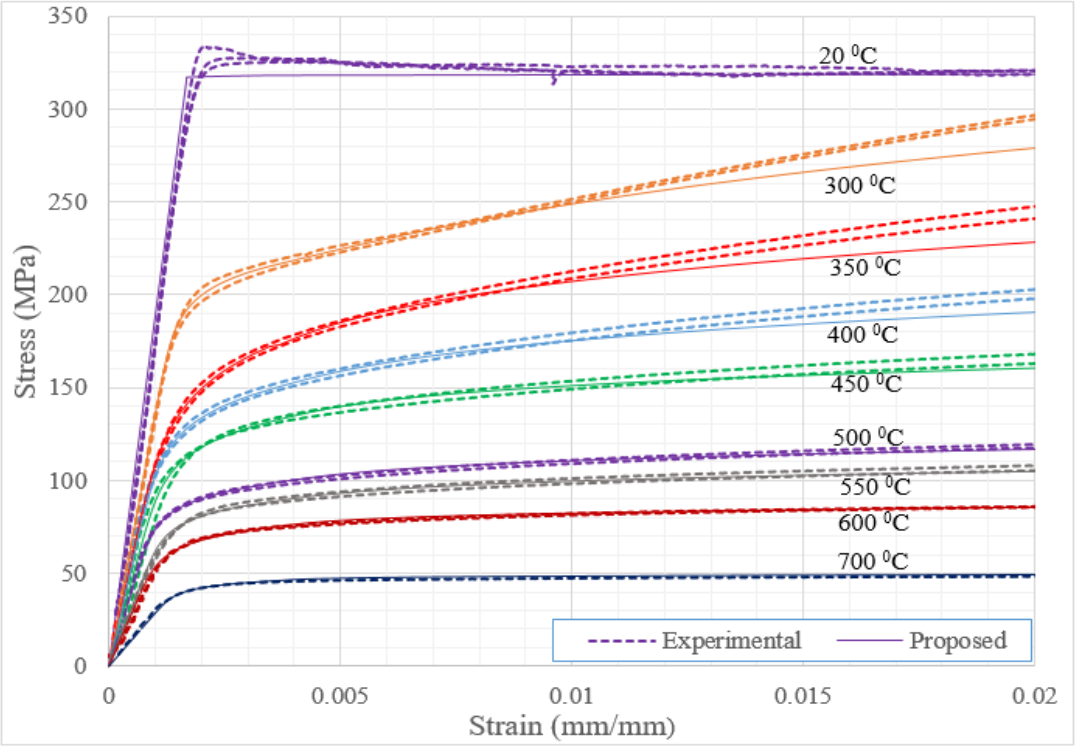

c. G300-1.0 mm cold-rolled steel sheet

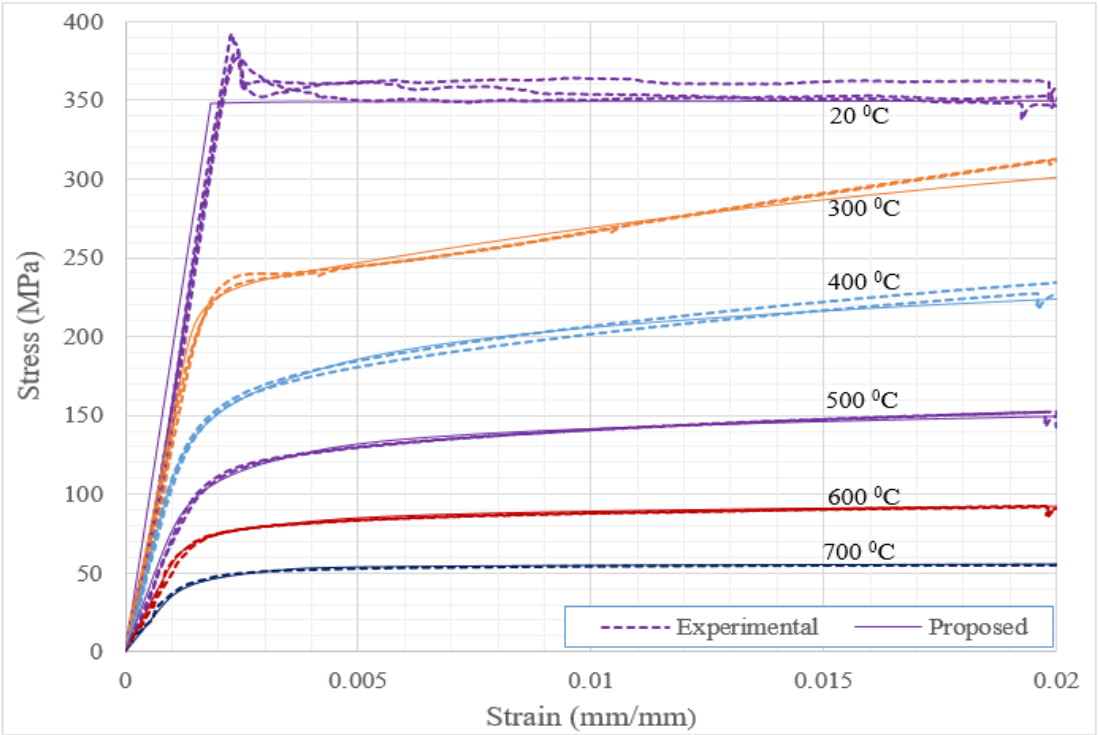

d. G300-0.8 mm cold-rolled steel sheet

Fig. 23. Comparison of stress-strain curves predicted by the proposed two-stage model with experimental stress-strain curves

4.5. Proportional limit stress to yield strength ratio

The proportional limit stresses can also be obtained approximately from the theoretical stress-strain curves developed using the mechanical properties obtained from the experimental stress-strain curves. Although the two-stage stress-strain models are developed based on a zero proportional limit stress, the proportional limit stress can be obtained visually (the stress at which the nonlinearity portion starts) since the deviation between the two-stage and perfect elastic stress-strain curves is negligible up to the proportional limit stress. Fig. 24 shows the proportional limit stress to yield strength ratios obtained from the experimental and proposed two-stage stress-strain curves (both visually). The proposed two-stage stress-strain model gives close predictions with those obtained from the experimental stress-strain curves.

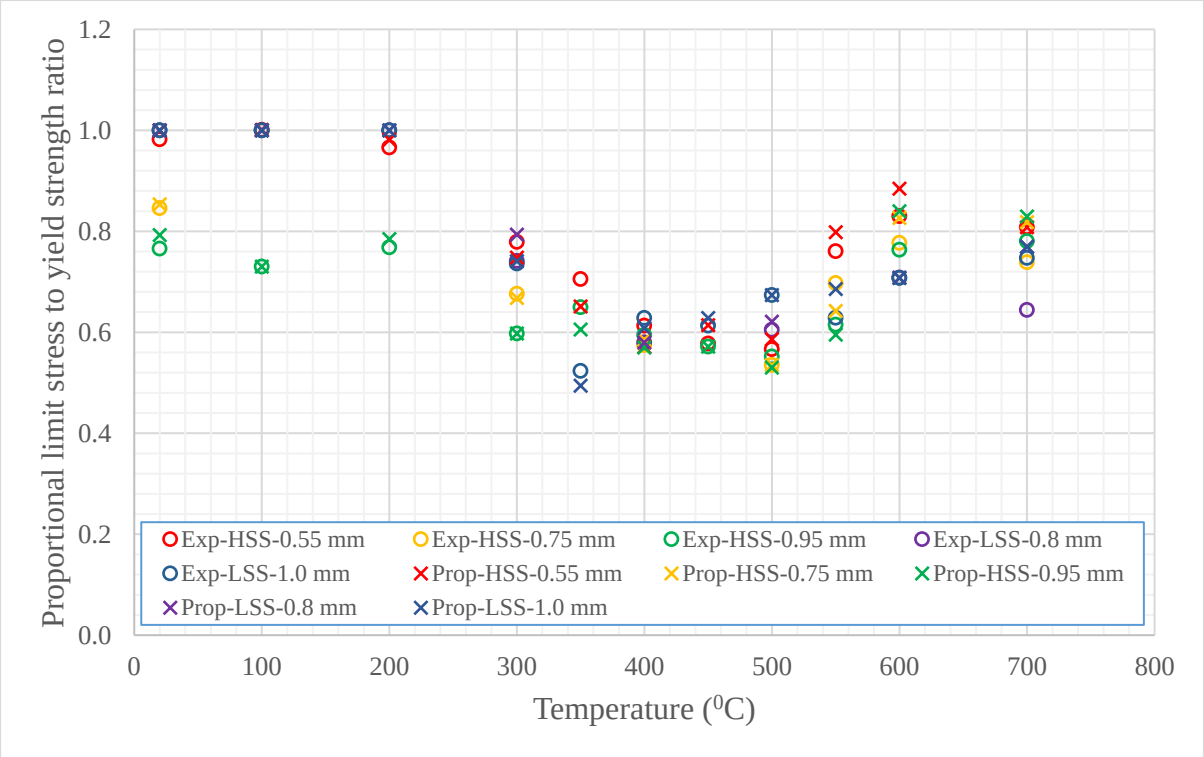

Fig. 24. Proportional limit stress to yield strength ratios obtained from the experimental and proposed stress-strain curves

5. Comparison of experimental results of cold-formed steel sections with the predictive equations developed for cold-rolled steel sheets

Ambient temperature mechanical properties and elevated temperature mechanical property reduction factors of cold-formed steel sections may differ from those of cold-rolled steel sheets due to the cold-forming process used. Generally, cold-forming process increases the ambient

temperature mechanical properties of cold-formed steel sections. However, it is not known whether the mechanical property reduction factors given in AS/NZS 4600 [9] and AS/NZS 2327 [10] derived based on the experimental results of cold-rolled steel sheets can be used for cold-formed steel sections such as lipped channel sections (LCS). Therefore tensile coupons extracted from the web and flange elements of cold-formed LCS and floor decks were tested at ambient and elevated temperatures, and their mechanical properties were determined.

The experimental results of LCS and floor decks, such as yield strength, Young's modulus, ultimate strength, stress at 2% total strain, 0.05% proof stress and proportional limit stress, were compared with the mechanical property reduction factor predictive equations developed for cold-rolled steel sheets in Fig. 25. Also, the average ultimate and fracture strains obtained for cold-rolled steel sheets were compared with those of LCS and floor decks in Figs. 26 and 27, respectively. These comparisons show that the elevated temperature reduction factor equations developed for cold-rolled steel sheets and the average ultimate and fracture strains obtained for cold-rolled steel sheets can be used for cold-formed steel LCS and floor decks safely. They show that the yield strength, stress at 2% total strain, ultimate strength, 0.05% proof stress and proportional limit stress of cold-formed steel sections are higher than those of cold-rolled steel sheets in the temperature range of 300 to 600 ^{0}C. Also, Fig. 28 compares the experimental stress-strain curves of CFS sections with those predicted by the proposed two-stage stress-strain model. It shows that the two-stage stress-strain model can be used for CFS sections.

The reduction factors for the yield strength, stress at 2% total strain, ultimate strength and 0.05% proof stress of the web and flange elements of 1.2 mm LCS are similar while those of the web element of 0.75 mm LCS are slightly lower than for 1.2 mm LCS. Also, the reduction factors of 1 mm floor deck and 0.75 mm web element of LCS have similar values while those of 0.75 mm floor deck are lower than 1 mm floor deck. These differences indicate the influence of cold-forming on the mechanical property reduction factors. However, the influence is not significant for the cold-formed LCS and floor decks used in this study.

On the other hand, Kesawan et al. [8] observed considerably higher yield strength reduction factors for web and flange elements of cold-formed steel hollow flange channel sections (HFCS) in comparison with those measured for cold-rolled steel sheets. Hollow flange elements which would have undergone higher levels of cold-forming retained higher mechanical properties than less cold-worked web elements. A recent study by Imran et al. [5] confirmed Kesawan et al.'s [8] findings through their elevated temperature tests of coupons

taken from cold-formed square and rectangular hollow sections. Therefore they proposed new predictive equations for their hollow sections [5, 8]. However, for open cold-formed steel sections such as LCS and floor decks with lower levels of cold-forming in comparison with closed sections, the predictive equations proposed in this paper for the elevated temperature mechanical property reduction factors of cold-rolled steel sheets can be used.

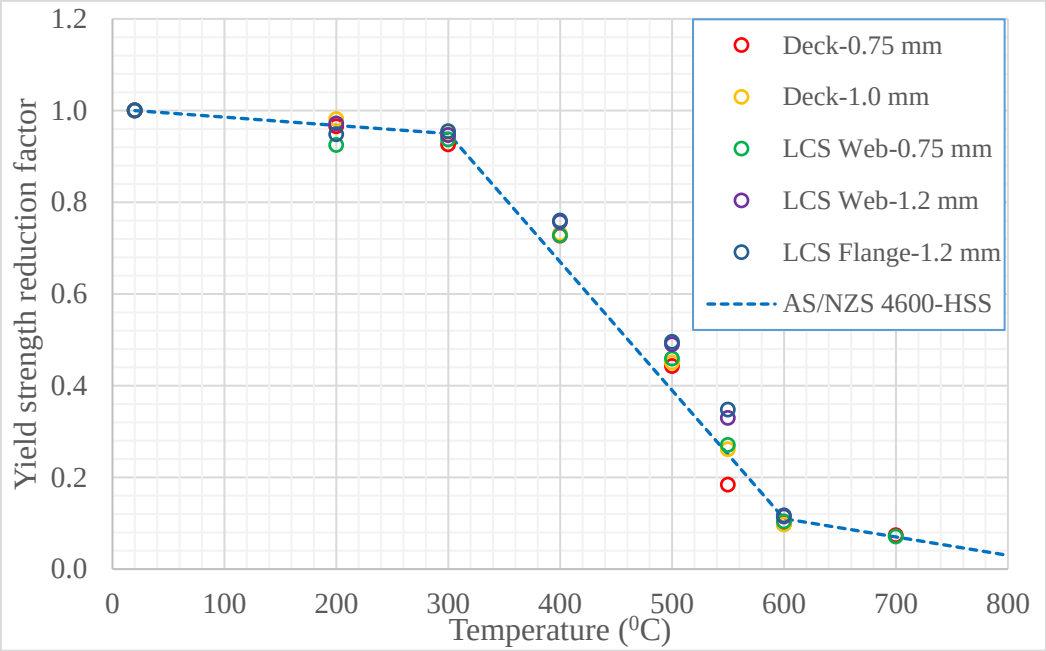

a. Yield strength reduction factors

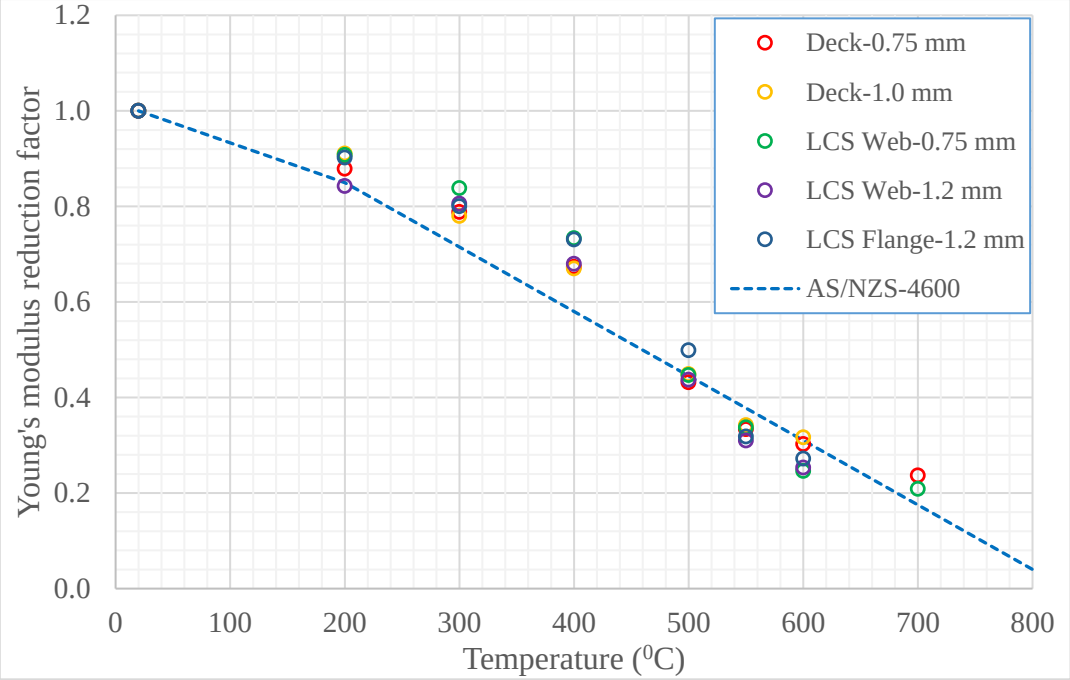

b. Young's modulus reduction factors

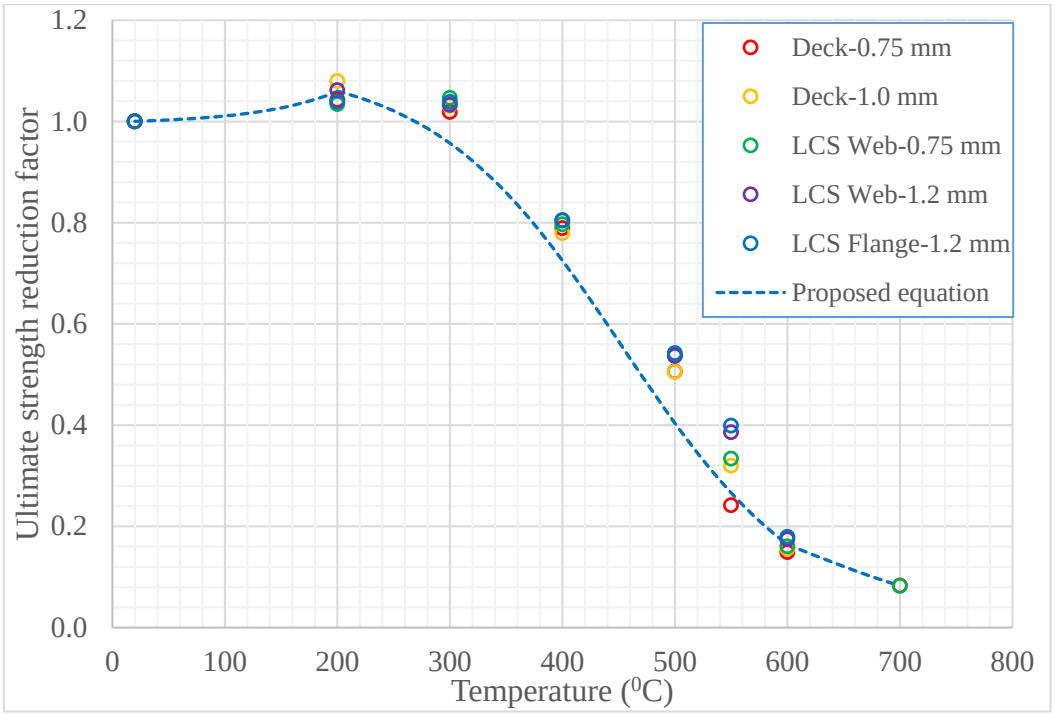

c. Ultimate strength reduction factors

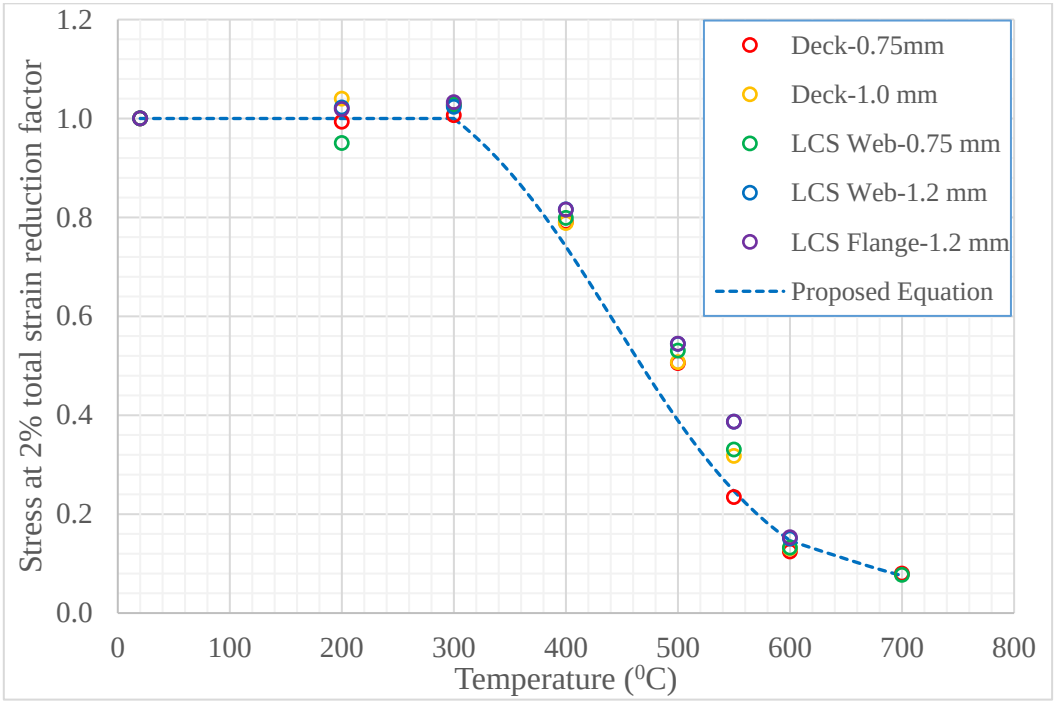

d. Stress at 2% total strain reduction factors

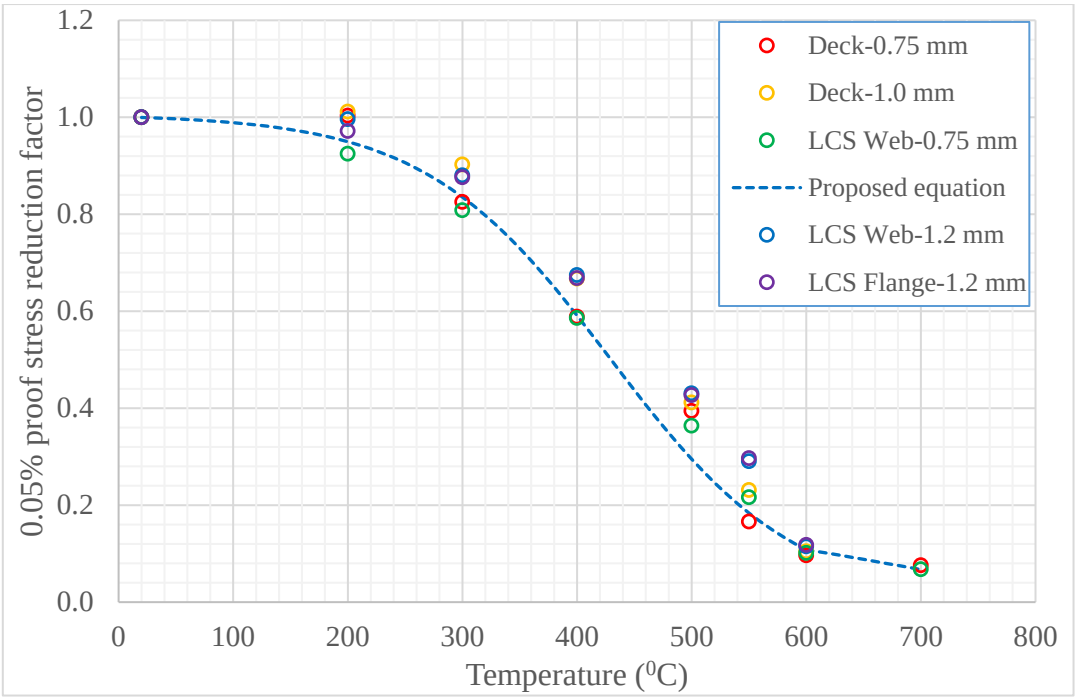

e. 0.05% proof stress reduction factors

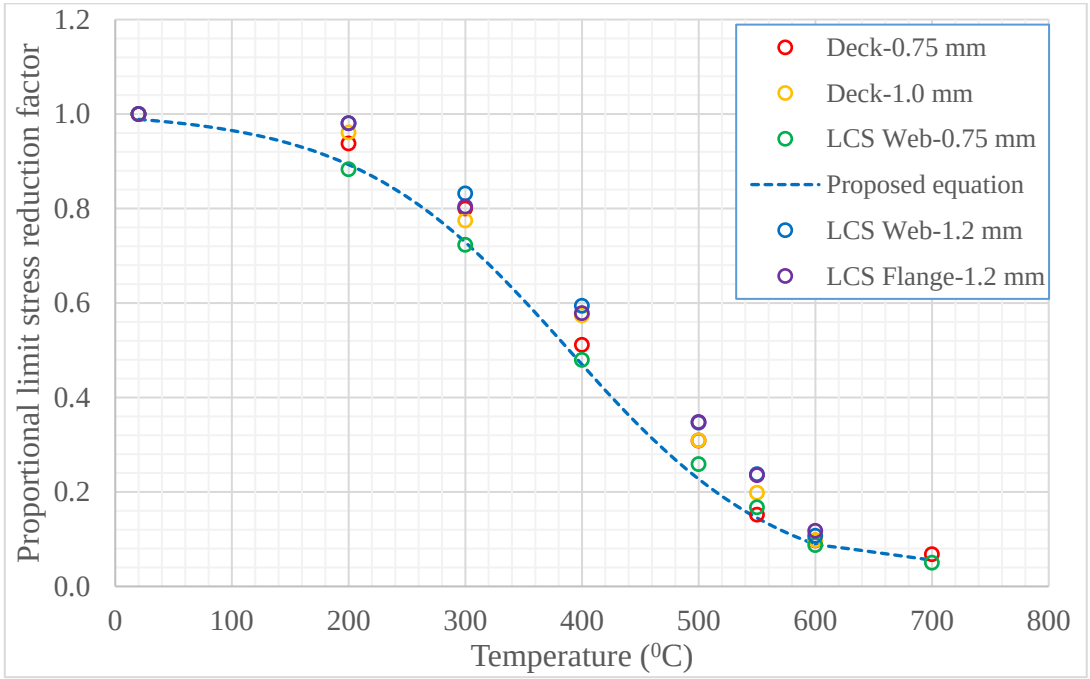

f. Proportional limit stress reduction factors

Fig. 25. Comparison of the proposed mechanical property reduction factor equations with experimental results of cold-formed steel sections

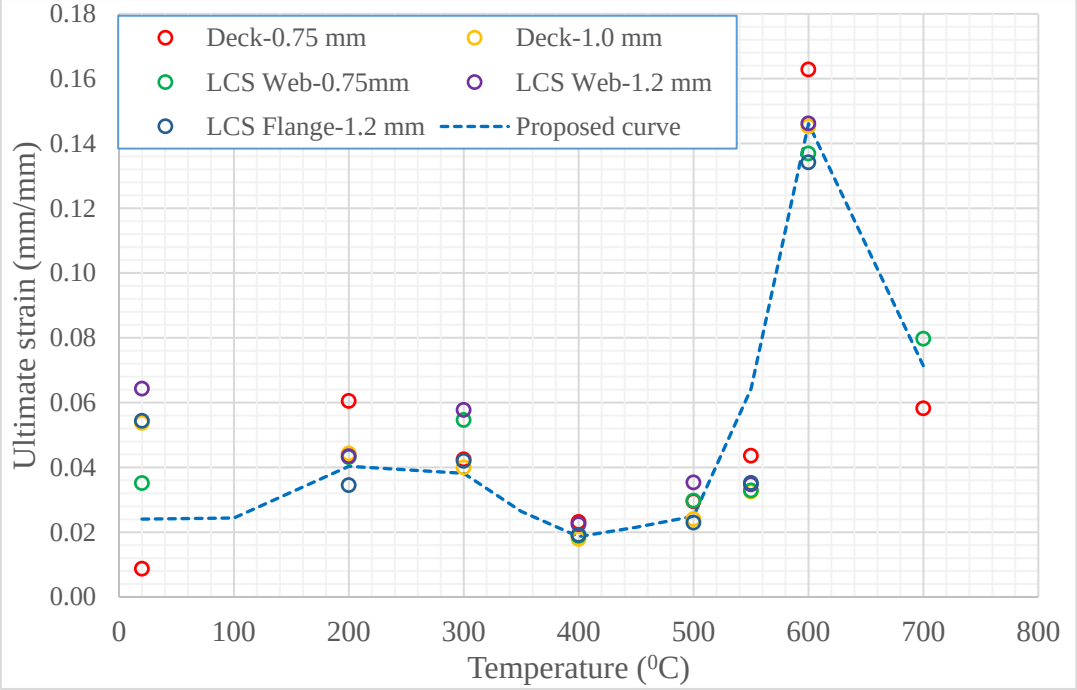

Fig. 26. Comparison of the average ultimate strains of cold-rolled steel sheets and cold-formed steel sections

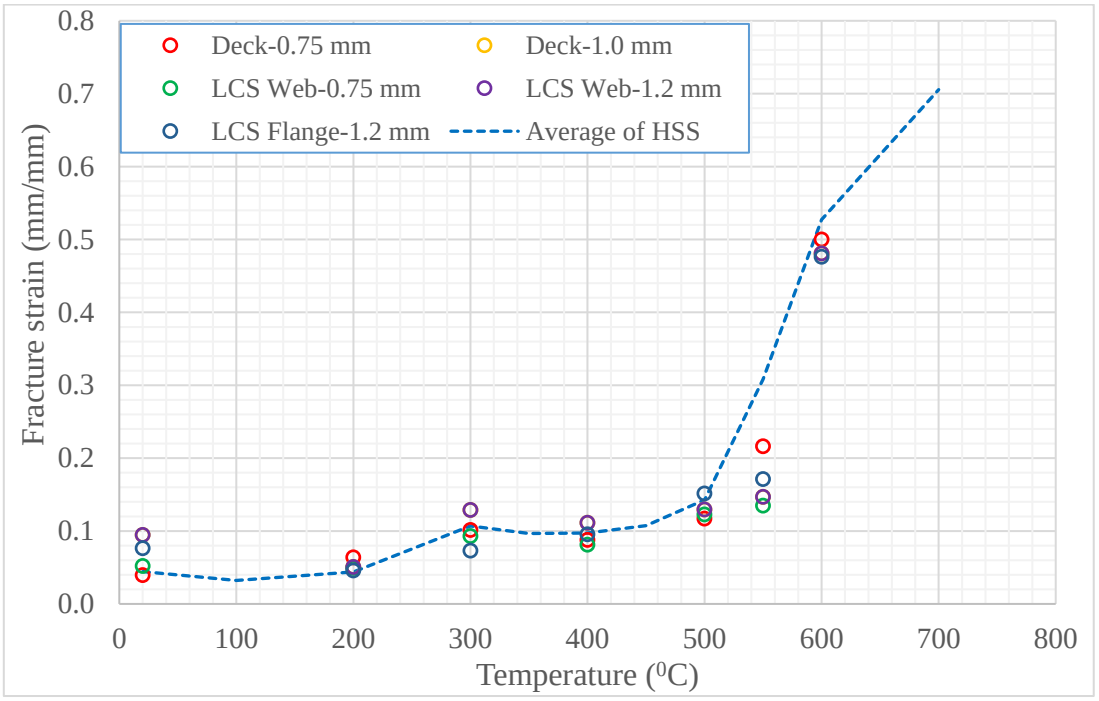

Fig. 27. Comparison of the average fracture strains of cold-rolled steel sheets and cold-formed steel sections

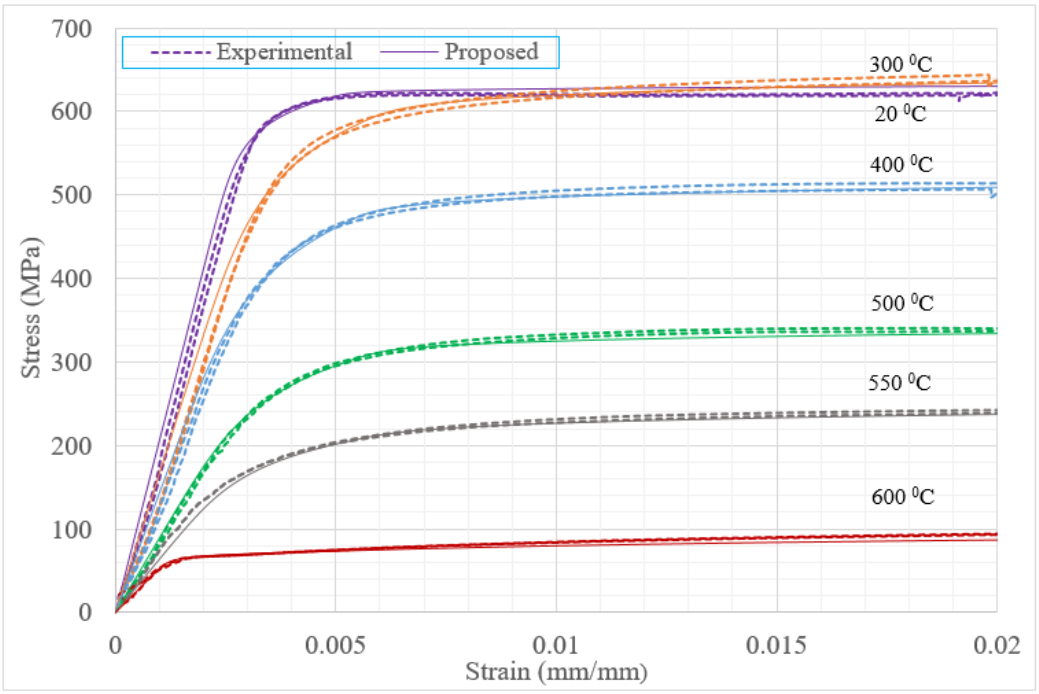

a. 1.2 mm LCS-web

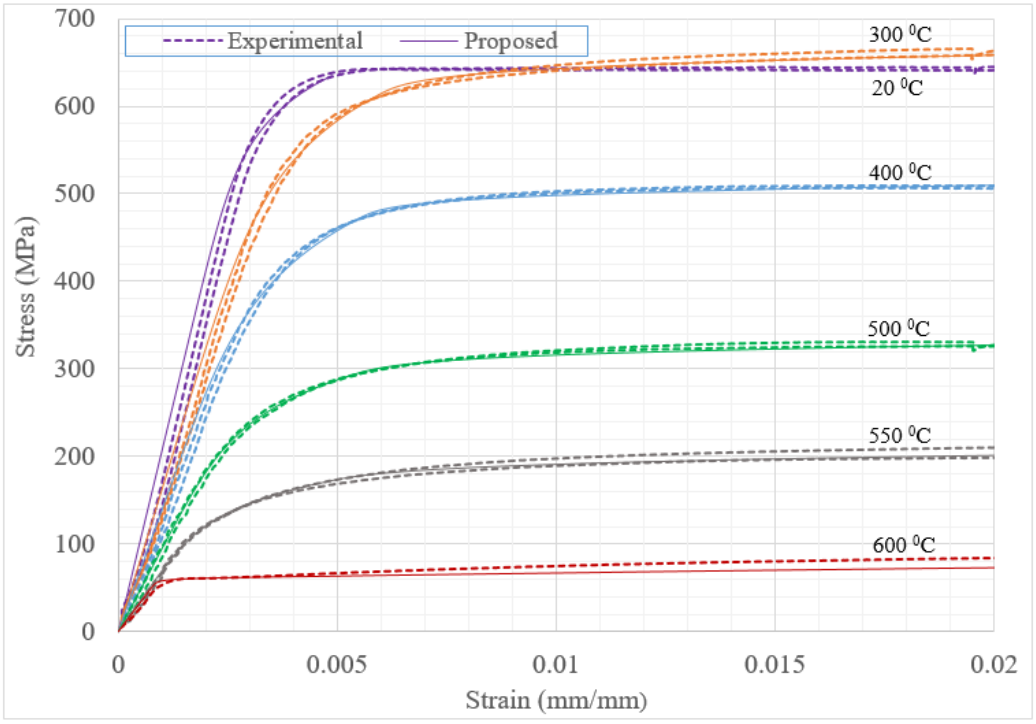

b. 1.0 mm floor deck

Fig. 28. Comparison of stress-strain curves predicted by the proposed two-stage model with experimental stress-strain curves of CFS sections

6. Comparison of experimental results of CFS lipped channel sections and floor decks with current design standards and past research papers

Elevated temperature mechanical properties predicted based on design standards and research papers hardly show any similarity among them. This could be due to many factors such as the variation of steel manufacturing process, level of cold-rolling and cold-forming, chemical composition, steel thickness, accuracy of elevated temperature testing facilities involving test set-up, test method and test measurements. In this section, predictive equations given in several design standards and research papers are compared with the experimental results of CFS lipped channel sections and floor decks. The yield strength and Young's modulus reduction factors of AS/NZS 2327 [10] for CFS are not plotted here as they are the same as in AS/NZS 4600 [9] for high strength CFS.

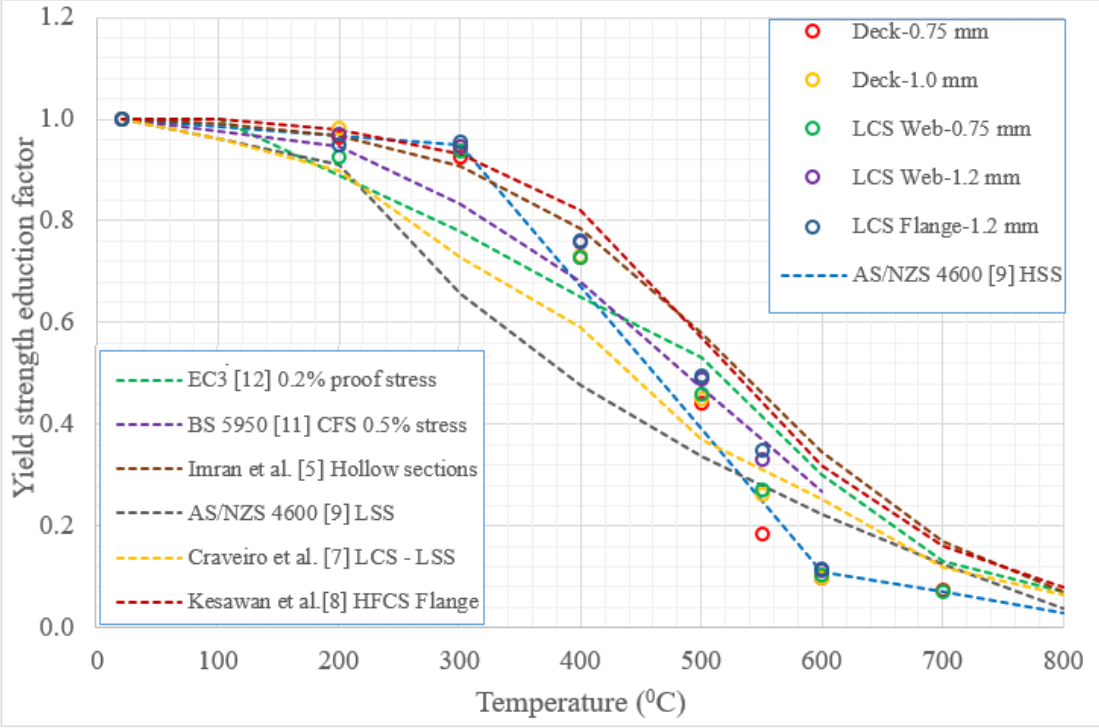

Fig. 29. Yield strength reduction factors of cold-formed steels given in design standards and research papers

Elevated temperature yield strength (0.2% proof stress) reduction factors of low and high strength CFS are compared in Fig. 29. BS 5950-Part 8 [11] does not provide 0.2% proof stress reduction factors. Therefore, stress at 0.5% strain, which is closer to 0.2% proof stress, was used. Elevated temperature yield strength reduction factors given in AS/NZS 4600 [9] for LSS, proposed based on cold-rolled steel sheets, are lower than those given in other design standards

and research papers at temperatures up to 500^0 C, whereas the yield strength reduction factors given in AS/NZS 4600 [9] for HSS are lower than those of LSS beyond 500^0 C. The reduction factors of Craveiro et al. [7] based on low strength CFS lipped channel sections are slightly higher than those of LSS given in AS/NZS 4600 [9]. This reduction factor increment is similar to that exhibited by high strength CFS lipped channel sections compared to the reduction factors of AS/NZS 4600 [9] for HSS cold-rolled sheets.

BS 5950-Part 8 [11] and Eurocode 3 Part 1-2 [12] show almost similar yield strength reduction factors, and fall between the reduction factors of CFS hollow sections and low strength CFS lipped channel sections. The yield strength reduction factors proposed by Kesawan et al. [8] for the web elements of hollow flange channel sections (HFCS) exactly match the Eurocode 3 Part 1-2 [12] reduction factors. Finally, the yield strength reduction factors proposed by Imran et al. [5] for CFS hollow sections and those proposed by Kesawan et al. [8] for the rectangular hollow flanges of HFCS are very similar. These variations in elevated temperature reduction factors clearly indicate the influence of section type on elevated temperature yield strength reduction factors as the level of cold-forming varies among cold-formed steel sections.

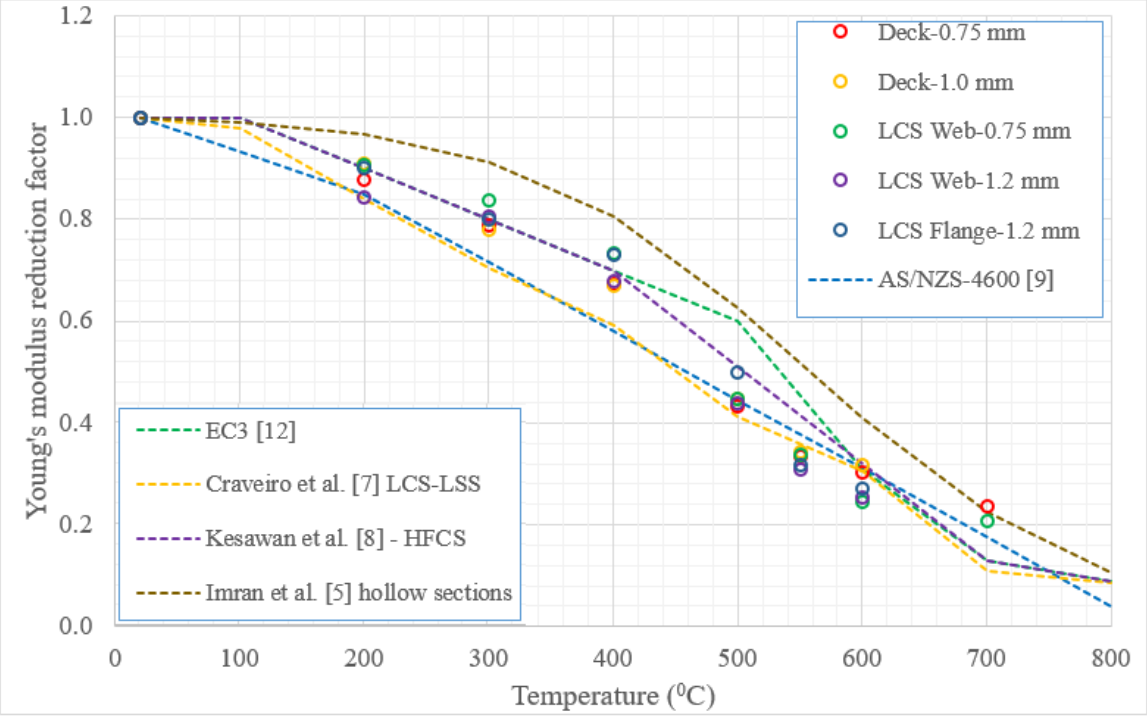

Fig. 30. Young's modulus reduction factors of cold-formed steels given in design standards and research papers

The elevated temperature reduction factors for Young's modulus in AS/NZS 4600 [9] and Craveiro et al. [7] are based on the experimental results of cold-rolled steel sheets and CFS channel sections, respectively, and they are almost similar as shown in Fig. 30. Kesawan et al.'s [8] results for HFCS and Eurocode 3 Part 1-2 [12] show almost similar reduction factors, which are higher than those of AS/NZS 4600 [9]. The Young's modulus reduction factors of CFS lipped channel sections and CFS floor decks tested in this study agree well with the AS/NZS 4600 [9] reduction factors although they fall closer to Eurocode 3 Part 1-2 [12] predictions at 300 and 400 ^{0}C. The Young's modulus reduction factors proposed by Imran et al. [5] for CFS hollow sections show the highest values among the reduction factors compared in this paper. These variations indicate the influence of the level of cold-forming. However, as seen in Figs. 29 and 30, the influence of cold-forming is less than that observed for yield strength reduction factors.

7. Conclusion

In this research, a detailed experimental study was conducted to determine the elevated temperature mechanical properties of cold-rolled steel sheets, cold-formed steel (CFS) channel sections and floor decks. Following are the main findings and recommendations from this research.

1. Experimentally determined elevated temperature mechanical properties of cold-rolled steel sheets such as yield strength and Young's modulus show a good agreement with the predictive equations of AS/NZS 4600 [9] and thus verify the accuracy of AS/NZS 4600 [9] equations in the fire designs of CFS structures. New predictive equations are proposed for the stress at 2% total strain, ultimate strength and 0.05% proof stress and proportional limit stress of cold-rolled steel sheets since AS/NZS 4600 [9] does not have them.
2. The AS/NZS 4600 [9] equations for the elevated temperature mechanical property reduction factors can be used safely for open CFS sections such as lipped channel sections and floor decks. Despite the higher elevated temperature mechanical property reduction factors of lipped channel sections and floor decks in the temperature range of 300 to 600 ^{0}C, it is recommended that the reduction factor equations in AS/NZS 4600 [9] are used in fire designs since the increments are small and can vary depending on

the level of cold-forming/working. However, engineers and designers can use higher reduction factors if elevated temperature test results are available.

3. For CFS sections with hollow flanges involving higher levels of cold-working, the elevated temperature mechanical property equations in AS/NZS 4600 [9] are too conservative. Suitable equations developed for such sections should be used, for example, Imran et al. [5] and Kesawan et al. [8].
4. The one-stage stress-strain model in AS/NZS 4600 [9] accurately predicts the stress-strain curves of low strength CFS at ambient and elevated temperatures except for 300 ^{0}C. However, it is not accurate for high strength CFS. The one-stage model exhibits a lower level of nonlinearity and strain hardening than experimental results. The accuracy of using the one-stage model for capacity predictions depends on the level of the influence of nonlinearity and strain hardening on the member capacities at elevated temperatures.
5. A two-stage model is proposed to accurately predict the stress-strain behaviour of CFS at elevated temperatures. Although it is more complicated than the one-stage model of AS/NZS 4600 [9], it is much simpler than multi-stage models.

References

[1] T. Ranawaka, M. Mahendran, Experimental study of the mechanical properties of light gauge cold-formed steels at elevated temperatures, Fire Safety Jornal 44 (2) (2009) 219-229.

[2] N.D. Kankanamge, M. Mahendran, Mechanical properties of cold-formed steels at elevated temperatures, Thin-Walled Structure 49 (1) (2011) 26-44.

[3] A. Landesmann, F.C.M.D Silva, E.D.M. Batista, Experimental investigation of the mechanical properties of ZAR-345 cold-formed steel at elevated temperatures, Material Research 17 (4) (2014) 1082-1091.

[4] F. McCann, L. Gardner, S. Kirk, Elevated temperature material properties of cold-formed steel hollow sections, Thin-Walled Struct. 90 (2015) 84-94.

[5] M. Imran, M. Mahendran, P. Keerthan, Mechanical properties of cold-formed steel tubular sections at elevated temperatures, Journal of Constructional Steel Research 143 (2018) 131-147.

[6] H.T. Li, B. Young, Material properties of cold-formed high strength steel at elevated temperatures, Thin-Walled Structures 115 (2017) 289-299.

[7] H.D. Craveiro, J. P. C. Rodrigues, A. Santiago, L. Laím, Review of the high temperature mechanical and thermal properties of the steels used in cold formed steel structures – The case of the S280 Gd+Z steel, Thin-Walled Structures 98 (2016) 154-168.

[8] S. Kesawan, V. Jatheeshan, M. Mahendran, Elevated temperature mechanical properties of hollow flange channel sections, Construction and Building Materials 87 (2015) 86-99.

[9] Standards Australia (SA), AS/NZS 4600, Cold-formed Steel Structures, Sydney, Australia, 2018.

[10] Standards Australia, (SA), AS/NZS 2327, Composite Structures - Composite Steel - Concrete, Sydney, Australia, 2017.

[11] British Standards (BSI), BS 5950.8, Structural Use of Steel Work in Building — Part 8: Code of Practice for Fire Resistant Design, British Standard Institution, London, UK 2003.

[12] EN 1993-1-2, Eurocode 3: Design of Steel Structures. Part 1–2: General Rules-Structural Fire Design, European Committee for Standardization, Brussels, 2005.

[13] N.D. Kankanamge, M. Mahendran, Behaviour and design of cold-formed steel beams subject to lateral–torsional buckling, Thin-Walled Structures 51 (2012) 25-38.

[14] W. Ramberg, W. Osgood, Description of stress-strain curves by three parameters, 1943

[15] L. Gardner, X. Yun, 2018, Description of stress-strain curves for cold-formed steels, Construction and Building Materials 189 (2018) 527-538.

[16] Standards Australia, (SA), AS 1391, Metallic Materials — Tensile Testing at Ambient temperature, Sydney, Australia, 2007.

[17] Standards Australia, (SA), AS 2291, Metallic Materials — Tensile Testing at Elevated temperatures, Sydney, Australia, 2007.

[18] W. Chen, Y. Jihong, Mechanical properties of G550 cold-formed steel under transient and steady state conditions, Journal of Constructional Steel Research 73 (2012) 1-11.

[19] J.M. Franssen, P.V. Real, Fire Design of Steel Structures: EC1: Actions on structures; Part 1-2: Actions on structure exposed to fire; EC3: Design of steel structures; Part 1-2: Structural fire design. John Wiley & Sons; 2016

[20] Standards Australia (SA), AS/NZS 4100, Steel Structures, Sydney, Australia, 1998.

[21] Y. Huang, B. Young, The art of coupon tests, Journal of Constructional Steel Research 96 (2014) 159-175.

[22] S. Afshan, L. Gardner, The continuous strength method for structural stainless steel design, Thin-Walled Structures 68 (2013) 42-49.

[23] M. Seif, L. Choe, J. Gross, W. Luecke, J. Main, D. McColskey, F. Sadek, J. Weigand, C. Zhang, Temperature-dependent material modeling for structural steels: formulation and application: US Department of Commerce, National Institute of Standards and Technology, 2016.

[24] X. Q. Wang, Z. Tao, M.K. Hassan, C. Hou, Stress-strain curves for high strength steel Bisalloy 80: Paper presented in the 25th Australian Conference on Mechanics of Structures and Materials, Brisbane, Australia, 2018.

[25] J.L. Holmquist, A. Nadai, A theoretical and experimental approach to the problem of collapse of deep-well casing, In Drilling and Production Practice, edited: American Petroleum Institute, 1939.

[26] E. Mirambell, E. Real, On the calculation of deflections in structural stainless steel beams: an experimental and numerical investigation, Journal of Constructional Steel Research 54 (1) (2000) 109-133.

[27] M. Macdonald, J. Rhodes, G.T. Taylor, Mechanical properties of stainless steel lipped channels, 2000.

[28] K.J.R. Rasmussen, Full-range stress-strain curves for stainless steel alloys, Journal of constructional steel research 59 (1) (2003) 47-61.

[29] A.H. Stang, H.L. Whittemore, (1935), Test of steel tower columns for the George Washington Bridge, Journal of Research of the National Bureau of Standards, 15 (1935) 317-339.

[30] M.E. Garlock, S. Selamet. 2010, Modeling and behaviour of steel plate connections subject to various fire scenarios, Journal of Structural Engineering 136 (7) (2010) 897